Food Chemistry: X 22 (2024) 101272

Contents lists available at ScienceDirect

Food Chemistry: X

journal homepage: www.sciencedirect.com/journal/food-chemistry-x

Effects of UV/H_2O_2 degradation on *Moringa oleifera* Lam. leaves polysaccharides: Composition, *in vitro* fermentation and prebiotic properties on gut microorganisms

Min Yang [a,b,c], Liang Tao [a,b,c,*], Zi-Lin Wang [a,b], Ling-Fei Li [a,b], Cun-Chao Zhao [a,d], Chong-Ying Shi [a,b], Jun Sheng [b,d], Yang Tian [b,c,d,e,*]

[a] College of Food Science and Technology, Yunnan Agricultural University, Kunming, China
[b] National Research and Development Professional Center for Moringa Processing Technology, Yunnan Agricultural University, Kunming, China
[c] Engineering Research Center of Development and Utilization of Food and Drug Homologous Resources, Ministry of Education, Yunnan Agricultural University, Kunming, China
[d] Yunnan Key Laboratory of Precision Nutrition and Personalized Food Manufacturing, Yunnan Agricultural University, Kunming, China
[e] PuEr University, Puer, China

ARTICLE INFO

Keywords:
Moringa oleifera Lam. leaves Polysaccharides
UV/H_2O_2 degradation
Antioxidant
Faecal fermentation
Gut microbiota

ABSTRACT

Moringa oleifera Lam. leaves are a new raw food material rich in polysaccharides. These polysaccharides exhibit various biological properties, including antioxidant, hypoglycemic and immunoregulatory effects. However, the use of *Moringa oleifera* Lam. leaves polysaccharides (MOLP) may be limited by their large molecular weight (M_W) and presence of numerous impurities, such as pigments. Research has indicated that degraded polysaccharides usually exhibit high biological activity because of changes in physical structure and chemical properties. In this study, we focused on the extraction of a degraded-modified fraction from MOLP using the Ultraviolet/ Hydrogen peroxide (UV/H_2O_2) method. Specifically, the physicochemical properties and glycosidic bond composition of a particular fraction (UV/H_2O_2 degraded *Moringa oleifera* Lam. leaves polysaccharides in 3 h called DMOLP-3) were investigated. In addition, *in vitro* simulated digestion experiments showed that DMOLP-3 was only partially degraded during gastrointestinal digestion, indicating that DMOLP-3 can be utilised by gut microorganisms. Furthermore, the prebiotic properties of MOLP and DMOLP-3 was studied using an *in vitro* faecal fermentation model. The results indicated that compared with MOLP, DMOLP-3 led to a decrease in both the colour and M_W of the polysaccharides. In addition, this model exhibited enhanced solubility and antioxidant capabilities while also influencing the surface morphology. Moreover, DMOLP-3 can facilitate the proliferation of advantageous microorganisms and enhance the synthesis of short-chain fatty acids (SCFAs). These results provide valuable insights into the utilization of bioactive components in *Moringa oleifera* Lam. leaves for the intestinal health.

Abbreviations: MOLP, *Moringa oleifera* Lam. leaves polysaccharides; H_2O_2, Hydrogen peroxide; UV, Ultraviolet; DMOLPs, UV/H_2O_2 degraded *Moringa oleifera* Lam. leaves polysaccharides with different times; DMOLP-3, UV/H_2O_2 degraded *Moringa oleifera* Lam. leaves polysaccharides in 3 h; Min, Minute; V_C, Vitamin C; UP water, Ultrapure water; M_W, Molecular weight; SCFAs, Short-chain fatty acids; HPGPC, High performance gel permeation chromatography; FT-IR, Fourier transform infrared; GC–MS, Gas chromatography-mass spectrometry; ABTS, 2,2′-azino-bis(3-ethylbenzothiazoline-6-sulfonic acid); DPPH, 2.2-diphenyl-picryl-hydrazyl radical; PDI, Polymer dispersity index; SEM, Scanning electron microscopy; AFM, Atomic force microscope analysis; TFA, Trifluoroacetic acid; PCoA, Principal coordinate analysis; LDA, Linear discriminant analysis; ROS, Reactive oxygen species; NO, Nitric oxide; IL-6, Interleukin-6; TNF-α, Tumour necrosis factor-α; NF-κB, Nuclear factor kappa-B; Fuc, Fucose; Rha, Rhamnose; Ara, Arabinose; GlcN, *N*-acetyl-D glucosamine; Gal, Galactose; Glc, Glucose; Xyl, Xylose; Man, Mannose; GalA, Galacturonic acid; GulA, guluronic acid; GlcA, glucuronic acid; ManA, Mannuronic acid.; Fru, Fructose; Rib, Ribose..

* Corresponding authors at: National Research and Development Professional Center for Moringa Processing Technology, Yunnan Agricultural University, Kunming, China.
E-mail addresses: taowuliang@163.com (L. Tao), tianyang1208@163.com (Y. Tian).

https://doi.org/10.1016/j.fochx.2024.101272
Received 21 November 2023; Received in revised form 24 February 2024; Accepted 6 March 2024
Available online 11 March 2024

1. Introduction

Moringa oleifera Lam. leaves which are abundant in tropical and subtropical regions, serve as a new raw food material (Ministry of Health, PRC, 2012; Document NO.19, http://www.nhc.gov.cn/) due to their remarkable abundance of active factors such as polysaccharides (Yang, Lin, & Zhao, 2023). Polysaccharides extracted from *Moringa oleifera* Lam. leaves exhibit diverse biological functions that are beneficial to human health (Yang et al., 2022). Our previous summary indicated that MOLP are rich in monosaccharides, of which galactose and rhamnose are the main components (Yang et al., 2022). MOLP also contain uronic acid structures that contribute to their antioxidant properties. Furthermore, these structures make them readily available to human gut microbes (He et al., 2018). In addition, MOLP with ranched chains can form a cross-linked network structure, which improves the hygroscopicity and water retention of polysaccharides (Raja, Bera, & Ray, 2016). Several studies have shown that MOLP with special branch structures can also exert immune activity; for instance, MOLP containing arabinose, glucose and galactose moieties and specific glycosidic bonds (1 → 3,6)-β-D-Gal*p*, (1 → 6)-β-D-Gal*p*, (1 → 5)-α-L-Ara*f* and T-α-L-Ara*f* can improve the immune response of RAW 264.7 cells and increase their pinocytosis capacity (Li et al., 2020). Similarly, Cui et al. (2019) demonstrated that MOLP with certain α-glycosidic bonds, such as α-Ara*f*, α-Gly, β-Gal*p*, α-Gal*p* and β-Gly, have the potential to enhance immune activity. Therefore, we speculated that polysaccharides may be important active factors in the biological function of *Moringa oleifera* Lam. Leaves, those functions including antioxidative effects, immune system regulation and antidiabetic effects (Ma, Ahmad, Zhang, Khan, & Muhammad, 2020). However, MOLP are characterised by a deep colour, large M_W, high content of pigment, and poor solubility, which may affect its bioavailability in the body and exert their biological function (Chen, Zhang, Huang, Fu, & Liu, 2017; Raja et al., 2016). Therefore, it is necessary to continue to find ways to gently modify the structure of MOLP to better demonstrate its biological activity.

The conventional degradation techniques commonly used for modification the structure of polysaccharides and enhancing their biological activity include acid hydrolysis, enzymatic hydrolysis, ultrasound treatment and microwave irradiation (Wang & Cheong, 2023). Some methods for modifying the structure of MOLP have been reported, for example, after MOLP has been treated with cellulase hydrolysis, high-temperature exposure, yeast fermentation, liquid nitrogen crushing, the results show that MOLP turns into white flakes, indicating that the treatments affect the MOLP structure too much, and the polysaccharide structure has been modified (Yang et al., 2023). Previous research has shown that degrading polysaccharides improves their physiological properties, increasing their effectiveness in oxidative stress, preventing bacterial growth, hypoglycemic and hypolipidemic effects (Abou Zeid, Aboutabl, Sleem, & El-Rafie, 2014; Zhou, Chen, Chen, & Chen, 2022). Currently, UV/H_2O_2 treatment is a novel and highly promising technique for degrading plant polysaccharides. This method offers various advantages, including accessibility, simple operation and utilization of mild environmental conditions (Chen, You, Ma, Zhao, & Kulikouskay, 2021). Many studies have reported that compared with original polysaccharides, UV/H_2O_2_degraded polysaccharides usually exhibit high biological activity due to their different structures and physicochemical properties (Chen et al., 2021; Gong et al., 2021). Compared with their original counterparts, the polysaccharides exhibited reduced toxicity in LPS-induced RAW 264.7 cells following UV/H_2O_2 treatment for 0.5–2 h (Chen et al., 2023). In recent years, the significant impact of natural plant polysaccharides as prebiotics on the gut microbiota has attracted increased amounts of attention (Yuan, Li, You, Dong, & Fu, 2020). MOLP have been reported to be prebiotics that regulate intestinal environmental health, but their complex structure may affect their function (Dou, Chen, & Fu, 2019; Gao et al., 2017). Recent studies have highlighted the importance of changes in polysaccharide structure for prebiotic activity, it has been observed that degradation of polysaccharides can improve their transport speed and absorption efficiency in the gastrointestinal system (Chen et al., 2020). Our early investigative studies showed that degradation of MOLP using UV/H_2O_2 (especially after 3 h) resulted in better antioxidant activity (production were not published).

In this study, MOLP were treated with different UV irradiation times combined with H_2O_2, and the compositions of the MOLP and DMOLP-3 were characterised, including their physical properties, M_W, monosaccharide composition, particle size potential and apparent morphology. Moreover, the type of glycosidic bond of DMOLP-3 was characterised. By conducting *in vitro* simulated gastrointestinal digestion experiments, we examined the changes in the molecular weight, monosaccharide composition and reducing sugars of DMOLP-3. By conducting *in vitro* faecal fermentation experiments, we examined the prebiotic properties of MOLP and DMOLP-3. The purpose of this study was to provide a theoretical basis for the use of MOLP as functional food materials to support intestinal health regulation.

2. Materials and methods

2.1. Chemicals and standards

The powdered of *Moringa oleifera* Lam. leaves were obtained from Tianyou Technology Co., Ltd. (Dehong, China). Hydrogen peroxide and manganese dioxide were obtained from Aladdin Technology Co., Ltd. (Shanghai, China). 2.2-diphenyl-picryl-hydrazyl radical (DPPH), 2,2′-azino-bis(3-ethylbenzothiazoline-6-sulfonic acid) (ABTS) and hydroxyl radical assay kits were purchased from Solarbio Technology Co., Ltd. (Beijing, China). Monosaccharide standards were obtained from BoRui Polyscilife Co., Ltd. (Jiang Su China). Sixteen kinds of monosaccharide standards (fucose, rhamnose, arabinose, galactose, glucose, xylose, mannose, fructose, ribose, galacturonic acid, glucuronic acid, galactosamine hydrochloride, glucosamine hydrochloride, *N*-acetyl-D glucosamine, guluronic acid and mannuronic acid) were prepared as standard stock solutions. All the chemical reagents were of analytical grade.

2.2. Methods for extracting MOLP and DMOLPs

DMOLPs, a degraded form of MOLP, were prepared following a previously established method with some adjustments (Chen, Sun-Waterhouse, et al., 2021). Briefly, MOLP were obtained by hot water extraction. The experimental setup involved placing 30 mL of the reaction solution, which consisted of MOLP and H_2O_2 at concentrations of 3.5 mg/mL and 300 mmol/L in a 90 mm glass petri dish, respectively, the solution was subjected to different incubation times (0 h, 0.5 h, 1 h, 1.5 h, 2 h, 2.5 h and 3 h) of UV irradiation after H_2O_2 treatment for different durations. The products were named as DMOLPs (including DMOLP-0.5 (0.5 h), DMOLP-1 (1 h), DMOLP-1.5 (1.5 h), DMOLP-2 (2 h), DMOLP-2.5 (2.5 h) and DMOLP-3 (3 h). To ensure the elimination of any residual H_2O_2, manganese dioxide was utilised. The obtained supernatant was concentrated through rotary evaporation, followed by freeze-drying to obtain DMOLPs. The preparation procedure is shown in Fig. 1A.

2.3. Analysis of the physical and chemical properties of polysaccharides

2.3.1. Colour analysis of MOLP and DMOLPs

A colourimeter (CR-400/410 Konica Minolta Investment Co., Ltd., China) was utilised to measure the colour of the polysaccharide sample. Prior to conducting the measurements, the colourimeter was calibrated using a white standard plate. To ensure the accuracy of the experiment, three samples were randomly chosen from each group, with 5 points selected from each sample for further analysis. A colorimetric measurement based on the study by Yang et al. (2023) assessed the brightness (L*), red/green (a*) and yellow/blue (b*) colour values.

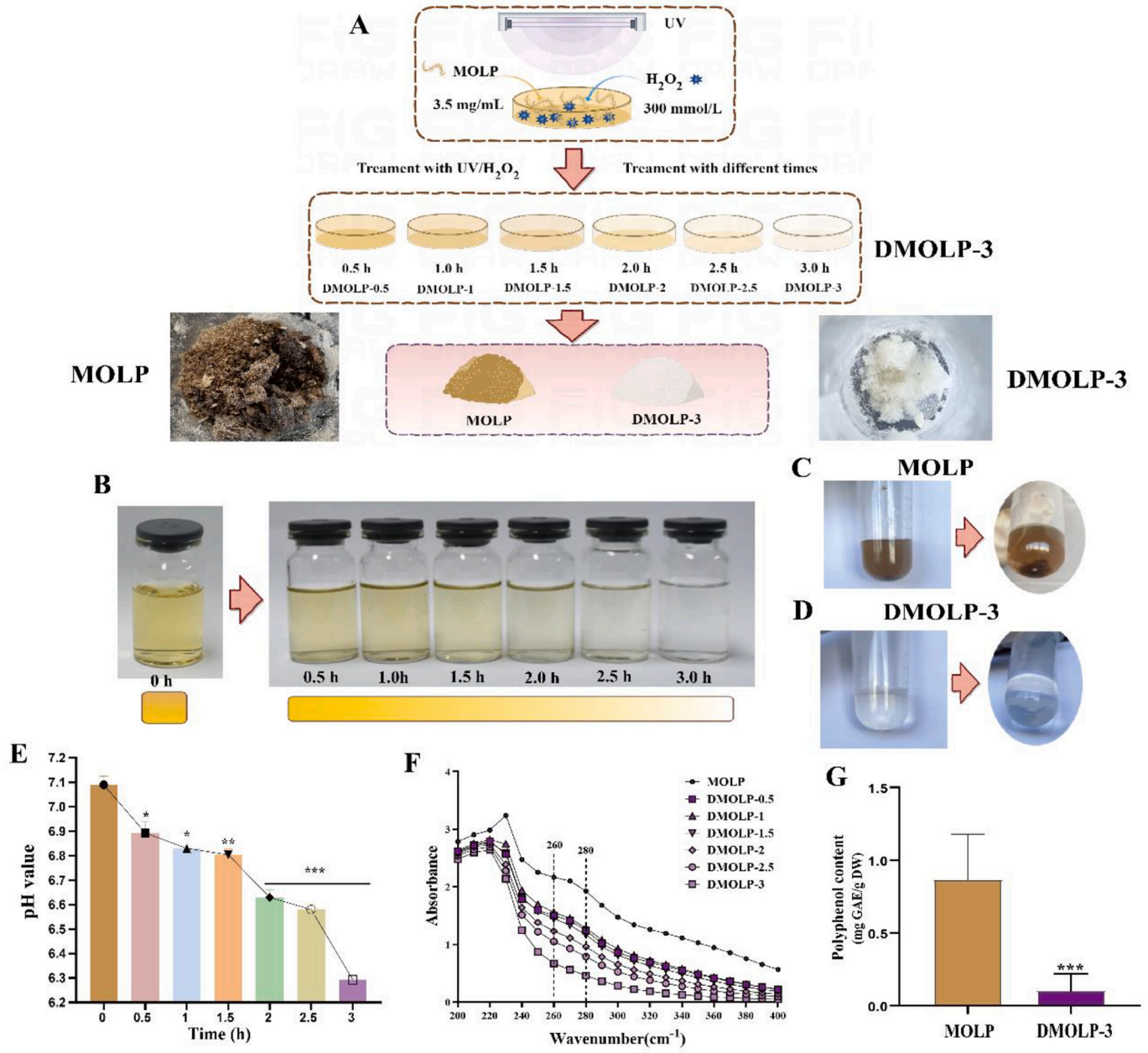

Fig. 1. Physicochemical properties of MOLP and DMOLPs (A). A schematic diagram of the sample preparation procedure; (B). Changes in the colour of MOLP and DMOLP-3 induced by UV/H_2O_2 treatment; (C). Changes in the solubility of MOLP induced by UV/H_2O_2 treatment; (D). Changes in the solubilities of DMOLP-3 induced by UV/H_2O_2 treatment; (E). Changes in the pH of MOLP and DMOLP-3 induced by UV/H_2O_2 treatment; (F). Changes in the ultraviolet spectrum of MOLP and DMOLP-3 induced by UV/H_2O_2 treatment; (G). The phenol content of MOLP and DMOLP-3.

2.3.2. *Solubility*

The colorimetric measurements were based on the study by Yu, Zhu, Xu, Wu, and Yu (2023). Polysaccharides (10 mg) were added to distilled water (2 mL) and stirred magnetically at room temperature for 1 h. The frontal dissolution of polysaccharides in water was observed and photographed.

2.3.3. *UV–vis scans of MOLP and DMOLPs*

Two milliliters of aqueous solutions of MOLP or DMOLPs (1.0 mg/mL) were prepared and scanned using a UV spectrophotometer (UV-2550, Shimadzu Corporation, Co., Ltd., Japan) in the wavelength range of 200–400 nm^{-1}.

2.3.4. *pH values of MOLP and DMOLPs*

The pH of the DMOLP$_S$ was measured with a pH meter (FE28, Mettler Toledo Co., Ltd., Switzerland). All measurements were performed in triplicate.

2.3.5. *Polyphenol content of MOLP and DMOLPs*

The total phenol content in the MOLP and DMOLP-3 was determined by the folin phenol method following the methods of Dengta, Banshtu, Verma, Gautam, and Sharma (2023). A diluted sample (0.5 mL) was added to a 10 mL tube, and 1.5 mL of Folin phenol reagent (0.25 mol/L) was added. Then, a 3 mL sodium carbonate solution (75 g/L) was added to the mixed solution, and ultrapure water was added to a fixed volume of 10 mL. The absorbance was measured at 760 nm^{-1} after the reaction had continued for 60 min, and the total phenol content was calculated using gallic acid as the standard.

2.3.6. Polysaccharide chemical composition analysis of MOLP and DMOLP

The contents of total carbohydrate content and uronic acid content were measured by using the phenol–sulfuric acid method and the carbazole-sulfuric acid method (Bitter & Muir, 1962). The reducing sugar content was assessed by the 3,5-dinitrosalicylic acid method, following a previously described method (Li, Dong, et al., 2020). The protein content was determined using a total protein assay kit (P0010, Beyotime Bioengineering Institute, Nanjing, Jiangsu Province, China). Reference standards such as glucose, bovine serum albumin and glucuronic acid were used for these tests.

2.3.7. Determination of the oxidation resistance of MOLP and DMOLP-3

DPPH radical scavenging capacity was determined according to the DPPH Free Radical Scavenging Capacity Assay Kit method (NO: BC4755), ABTS was determined according to the ABTS Free Radical Scavenging Capacity Assay Kit (NO: BC4775), and Hydroxyl Free Radical was determined according to the Micro Hydroxyl Free Radical Scavenging Capacity Assay Kit method (NO: BC1325). All kits were purchased from Solarbio Technology Co., Ltd. (Beijing, China). The radical scavenging activity values are expressed as IC_{50} values (mg/mL), the concentration needed for 50% radical inhibition by MOLP, DMOLP-3 or Vitamin C (V_C).

2.3.8. Determination of the M_w of MOLP and DMOLP-3

The M_W of the compound was successfully determined using High-performance gel permeation chromatography (HPGPC). For the analysis a HPGPC tandem gel column BRT105-104-102 (8 mm × 300 mm, BoRui Saccharide Biotech, China) and a refractive differential detector (RID-10A) were used in this research. The choice of a 0.2 M NaCl solution as the mobile phase, a flow rate of 0.8 mL/min, a column temperature of 40 °C, a 25 μL injection volume and an analysis time of 60 min provided optimal conditions for accurate measurements.

2.3.9. Determination of the monosaccharide composition of MOLP and DMOLP-3

An ion chromatography column Dionex CarbopacTM PA20 (3 × 150 mm, Dionex Corp. Sunnyvale, CA, USA) and a refractive differential detector were used for the determination of monosaccharide composition. MOLP (5 mg) and DMOLP-3 (5 mg) were placed in ampoule bottles, and 2 mL of 3-M trifluoroacetic acid (TFA) was added, the mixture was hydrolysed at 120 °C for 3 h. The acid hydrolysis solution was accurately absorbed and transferred to a tube for drying with nitrogen. Then, 5 mL of water was added, and the mixture was vortexed. A 50 μL sample was absorbed, and 950 μL of deionised water was added to bring the volume to 1 mL. The mixture was then centrifuged at 12,000 rpm for 5 min. The supernatant was collected for analysis. The composition of the mobile phase included deionised water (A), NaOH at a concentration of 15 mM (B), a combination of NaOH at 15 mM and NaOAc at 100 mM (C). The gradient was programmed as follows: at 0 min, the ratio of A:B:C was 98.8:1.2:0 (*V*/V) at 18 min, it was adjusted to 98.8:1 (V/V) at 20 min, and the ratio was changed to A:B:C50:50:0 (V/V); at 30 min, the ratio was adjusted to be the same as that at A:B:C50:50:0 (V/V); and at 46 min, the composition was shifted to A:B:C0:0:100 (V/V). In this experiment, the column temperature was set at 30 °C. The flow rate used was 0.3 mL/min, and the injection volume was 25 μL.

2.4. Analysis of the composition characteristics of polysaccharides

2.4.1. Fourier transform infrared (FT-IR) of MOLP and DMOLP-3

A mixture of polysaccharide and spectral-grade potassium bromide powder was pressed into a microsphere, and its FT-IR spectrum was recorded in the range of 400–4000 cm^{-1} using an FT-IR spectrophotometer (FT-IR650, Tianjin Port East Science and Technology Development Co., Ltd., China).

2.4.2. Congo red

According to the method of Feng et al. (2022), 2.0 mg of dry polysaccharide sample was accurately weighed, dissolved in 2.0 mL of ultrapure water (UP water), and 100 μmol/L Congo red reagent was added, after which 0 mol/L, 0.05 mol/L, 0.1 mol/L, 0.15 mol/L, 0.2 mol/L, 0.25 mol/L, 0.3 mol/L 0.35 mol/L, 0.4 mol/L, 0.45 mol/L and 0.5 mol/L were added in sequence. The NaOH solution was mixed evenly and allowed to stand at room temperature for 20 min. A UV spectrophotometer (UV-2550, Shimadzu Corporation, Co., Ltd., Japan) was used to measure the maximum absorption wavelength of Congo red in NaOH solutions of different concentrations, with a scanning range of 400–600 nm^{-1}.

2.4.3. Scanning Electronic Microscopy (SEM) of MOLP and DMOLP-3

SEM was employed to characterise the surface morphology and microstructure of the MOLP and DMOLP-3 (EVO 18, Carl Zeiss, Baden-Württemberg, Germany). Under a vacuum accelerating voltage of 10 kV, the freeze-dried polysaccharides were examined after being coated with a delicate gold layer.

2.4.4. The Zeta potential of MOLP and DMOLP-3

The zeta potentials of the samples were measured by using a nanoparticle size potentiometer (Malvern Zetasizer Nano ZS90, Malvern, UK). Before the assay, each group of samples was diluted 100-fold with distilled water. The average zeta potential was calculated based on three parallel measurements.

2.4.5. Atomic force microscope (AFM) of MOLP and DMOLP-3

Atomic force microscope (AFM) (Bruker, Santa Barbara, CA, Germany) was used to observe the surface morphology and roughness of the MOLP and DMOLP-3. First, the polysaccharide was completely dissolved in distilled water at a concentration of 0.01 μg/mL. Subsequently, the solution was filtered through a 0.22 μm filter membrane. Next, a freshly cracked mica plate was chosen as the substrate, and 2 μL of the solution was carefully transferred onto it. The plate was then left to dry overnight at room temperature. The controller was used to capture AFM images, which were subsequently processed using the Nanoscop scanning image processor software (version 6.7.8, Denmark).

2.4.6. Methylation analysis of DMOLP-3

Methylation of DMOLP-3 was performed using a previously described method (Hui et al., 2023). In this method, methylated polysaccharide samples are first hydrolysed with 2 M trifluoroacetic acid (TFA) for 90 min. The samples are subsequently reduced with $NaBH_4$ for 8 h. Then, acetic anhydride was added and the acetylation reaction was performed at 100 °C for 1 h. The products were then extracted with CH_2Cl_2 and extracted with Na_2SO_4, after which the products were determined by Gas chromatography-mass spectrometry (GC–MS) (6890–5973, Agilent, USA). For GC–MS analysis a SIL Rsi-5 column (dimensions 30 m × 0.25 mm × 0.25 μm) was used. Helium was used as carrier gas at a flow rate of 1 mL/min. The inlet temperature was 250 °C, and the detector temperature was 250 °C. The heating process was as follows: both the initial and detector temperatures were set to 250 °C. The heating process started at an initial temperature of 120 °C and then increased to 250 °C at a rate of 3 °C/min, after which the temperature was maintained for 5 min.

2.5. In vitro simulated gastrointestinal digestion of DMOLP-3

To evaluate the stability of the digestive process of DMOLP-3, *in vitro* gastrointestinal digestion was performed based on previously reported methods (Minekus et al., 2014) with minor modifications. The simulated digestion steps were as follows:

2.5.1. Oral salivary digestion

DMOLP-3 (1 g) was dissolved in simulated saliva, after which

α-amylase (3700 U/mg) and 25 μL of $CaCl_2$ solution (0.3 mM) were added. Subsequently, 10 mL of ultrapure water was added, and the mixture was incubated at 37 °C for 2 min.

2.5.2. Gastric digestion

An 8 mL gastric digestive reserve solution, 0.42 mL of pepsin (2000 U/mL) and 27.5 μL of $CaCl_2$ solution (44.1 g/L) were added to the oral digestion mixture; the pH was adjusted to 3.0, and adjusted to a final volume of 10 mL with ultrapure water. After fully mixing, the mixture was placed in a thermostat shaker in the dark and shaken at 37 °C for 2 h.

2.5.3. Intestinal digestive tract

Then, 2.5 mL of pepsin (2000 U/mg), 1.5 mL of bile salt (200 mg/mL) and 20 μL of $CaCl_2$ solution were added to the intestinal digestive fluid, the pH was adjusted to 7.0, the supplemented ultrapure water was fixed to 20 mL, and the mixture was thoroughly mixed and placed on a shaking table at 37 °C in the dark and shaken for 2 h. The mixture was centrifuged at 4 °C (10,000 r/min) for 10 min and boiled in a water bath at 100 °C for 5 min to inactivate the enzymes. The supernatant was dialysed in ultrapure water (dialysis bag M_W cut-off 500 Da), freeze-dried and named DMOLP-3I.

2.6. In vitro faecal fermentation of MOLP and DMOLP-3

In vitro faecal fermentation of MOLP and DMOLP-3 was conducted using a method previously described by Tan et al. (2020), with few modifications. Faecal samples were obtained from a total of four human participants (two men and two women). These individuals had not been subjected to any antibiotic treatments in the previous 6 months, and they also adhered to similar dietary patterns and environmental conditions. Thus, the faecal materials collected were relatively standardised and comparable. The faecal samples were blended with phosphate buffer (32%, *w/v*) and promptly agitated. The surplus bulky food particles in the faecal mixture were eliminated through centrifugation at 265 ×*g* for 5 min, and the resulting liquid was utilised as the slurry for subsequent investigations. Three sets of fermentation experiments resembling *in vitro* conditions were formulated, encompassing two experimental groups (MOLP and DMOLP-3) and a control group without any additional carbon sources. The samples that underwent fermentation for 24 h were promptly extracted for additional analysis, with each trial being replicated four times.

2.6.1. Determination of the gut microbiota by 16S rRNA after MOLP and DMOLP-3 fermentation

A DNA Kit (Omega Biotek, Norcross, GA, USA) was utilised to extract the overall DNA of the intestinal gut microbiota in all the experimental groups. Following the extraction process, the purity and concentration of the DNA samples were assessed using a NanoDrop 2000 nucleic acid protein spectrophotometer (Thermo Scientific, USA). After purification and quantification, Majorbio Bio-Pharm Technology Co., Ltd. (Shanghai, China) sequenced the gut microbiota using the Illumina MiSeq PE300 platform for sample analysis. The amplification of the bacterial communities was performed by selecting the region of the 16S rRNA gene. Subsequently, the sequenced 16S amplicons were analysed using QIIME software. Furthermore, R software was used to analyse the differences in beta diversity between groups. A Principal coordinate analysis (PCoA) based on unweighted UniFrac distances was used to evaluate beta diversity. LEfSe software was used with a default Linear discriminant analysis (LDA) score filter value of 2.

2.6.2. Determination of SCFAs after MOLP and DMOLP-3 fermentation

2.6.2.1. SCFA extraction. A 25 mg solid sample was accurately weighed into a 2 mL grinding tube, and 500 μL of water containing 0.5% phosphoric acid was added. The sample was frozen and ground at 50 Hz for 3 min, which was repeated twice, followed by ultrasonication for 10 min and centrifugation at 4 °C and 13,000 × g for 15 min. Afterwards, 200 μL of the aqueous mixture was removed from the 1.5-mL centrifuge tube, after which 0.2 mL of N-butanol solvent containing the internal standard 2-ethylbutyric acid (10 μg/mL) was added for extraction. Finally, the sample was vortexed for 10 s, ultrasonicated at low temperature for 10 min, and then centrifuged at 4 °C and 13,000 × *g* for 5 min, after which the supernatant was carefully transferred to sample vials for analysis.

2.6.2.2. GC–MS analysis. The analysis was performed using an Agilent 7890B gas chromatograph coupled to an Agilent 5977B/7000D mass selective detector with an inert electron impact ionisation source, and the ionisation voltage was 70 eV (Agilent, USA) at Majorbio Bio-Pharm Technology Co. Ltd. (Shanghai, China). For GC–MS analysis a HP-FFAP column (dimensions 30 m × 0.25 mm × 0.25 μm) was used. The GC column temperature was programmed to hold at 80 °C and then gradually increase to 120 °C at a rate of 40 °C/min, then slowly increase to 200 °C at a rate of 5 °C/min and finally hold at a temperature of 220 °C for 3 min. The injection volume of the samples was 1 μL, and the samples were introduced in splitting mode (10:1) with an inlet temperature of 180 °C. The ion source temperature was 230 °C, and the quadrupole temperature was 150 °C.

2.7. Statistical analysis

GraphPad Prism 7.0 was used to analyse the experimental data. The mean ± standard error of the mean was used to express the values. Student's *t*-test was used to compare the results. Each experiment was repeated in triplicate. Statistical significance was denoted as $^{*}P < 0.05$, $^{**}P < 0.01$ and $^{***}P < 0.001$, while $^{\#}P < 0.05$, $^{\#\#}P < 0.01$ and $^{\#\#\#}P < 0.001$ indicated substantial differences.

3. Results

3.1. Physicochemical properties of MOLP and DMOLPs

MOLPs were treated with UV and H_2O_2 for various times (0 h, 0.5 h, 1 h, 1.5 h, 1.5 h, 2 h, 2.5 h, and 3 h), and we found that these treatments effectively decolorized the MOLPs (Fig. 1A-B). The MOLP powder was dark and brown, whereas after UV/H_2O_2 treatment, the decolorization effect of the MOLP gradually increased and the DMOLP-3 powder was close to white, the colour change could be due to the degradation of phenolic compounds or proteins (Fig. 1A-B).

In addition, DMOLP-3 exhibited superior solubility compared with MOLP (Fig. 1-D). The reason for this difference may be that the treatments probably reduce the M_w, and also correlates with the increase in solubility as well as the treatment with H_2O_2, which most causes modifications that improve solubility. Yao et al. (2022) reported that seaweed polysaccharides have a high M_W and poor solubility, which limits their function and application. However, UV/H_2O_2 treatment can effectively degrade seaweed polysaccharides. After 2 h treatment, the M_W decreased from 271 kDa to 26 kDa, considerably improving the solubility. In addition, the H_2O_2 oxidation method is commonly used in the preparation of degraded polysaccharides because this method is less destructive to polysaccharides structures, and degraded polysaccharides exhibit better water solubility and biological function than original polysaccharides. Hou et al. (2012) used H_2O_2 to degrade *fucoidan* polysaccharides, and H_2O_2 can generate active free radicals that promote oxidation reactions. Moreover, Ma et al. (2022) reported that the tight triple helical structure and high M_W of yeast β-glucan lead to its insolubility, which affects its biological activity and application range. Ultrasound-assisted H_2O_2 treatment can considerably improve the solubility of these materials. The difference in colour between MOLP and

DMOLPs in Table S1 also suggested the same results. Furthermore, the treatment duration exhibited a correlation with the decreasing trend of MOLP pH (Fig. 1E). The primary reason behind this pH decrease can be ascribed to the breakdown of glycosidic bonds within MOLP, which is induced by the presence of free radicals. The rate of change in pH during the irregular cleavage of glycosidic bonds to release uronic acid is initially rapid and then slows, this change may be attributed to the variations in the content of hydroxyl radicals in the reaction system (Chen, Sun-Waterhouse, et al., 2021; Gong et al., 2021).

Several studies have shown that the deep colour of polysaccharides is caused by pigments, which may interfere the polysaccharides structural analysis and biological activity (Yuan, Zhong, & Liu, 2020). Ultraviolet spectrum analysis (200–400 nm^{-1}) also indicated that MOLP and DMOLP had characteristic absorption polysaccharides peaks at 220–230 nm^{-1}. The absorption peaks at 260–280 nm^{-1} indicated that there were still certain nucleic acids and proteins in the MOLP, and the signal above 300 nm^{-1} revealed that a large amount of pigment was present in the MOLP. However, after UV/H_2O_2 treatment, the nucleic acid and protein band at 260–280 nm^{-1} and most of the pigment bands after 300 nm^{-1} gradually became flat (Fig. 1F), indicating that degradation treatment may played a role in decolorization and deproteinization. Moreover, polyphenols also affect the determination of the ultraviolet spectrum at 280 nm^{-1} (Raal et al., 2012), so we evaluated polyphenol content in MOLP and DMOLPs, the results showed that compared with MOLP, the polyphenol content of DMOLP-3 was considerably lower after UV/H_2O_2 treatment.

3.2. Chemical composition of MOLP and DMOLP-3

Our previous studies have revealed that DMOLPs (especially DMOLP-3) exhibited better antioxidant properties (production were not published). Therefore, this study investigated the changes between MOLP and DMOLP-3. The chemical compositions of the MOLP and DMOLP-3 are showed in Table 1. After UV/H_2O_2 degradation, compared with MOLP, DMOLP-3 showed an increase in total carbohydrate contents and uronic acid contents. Similar studies have shown that the total carbohydrate content of seaweed polysaccharides from *Sargassum fusiforme* increased after UV/H_2O_2 treatment, possibly because UV/H_2O_2 treatment decomposes pigments and other impurities in polysaccharides, thereby increasing the efficiency of structural modification (Yao et al., 2022). Furthermore, Xu et al. (2019) used Fe^{2+} combined with H_2O_2 to treat raspberry fruit polysaccharides. The total carbohydrate content of the crude polysaccharides was 42.39% ± 1.14%, and the total carbohydrate content of the degraded polysaccharides was 46.74% ± 0.87%. Ma et al. (2021) also used V_C and H_2O_2 to prepare degradable polysaccharides from blue honeysuckle polysaccharides. The results showed that the total carbohydrate content of the degraded polysaccharide increased slightly, but the galacturonic acid content was significantly greater than that of the original polysaccharide. This difference may be due to the V_C/H_2O_2-induced chain scission in the polymer, which further releases galacturonic acid. These studies demonstrate that H_2O_2 treatment is an environmentally friendly method for modified polysaccharides by removing most impurities without significantly changing the basic polysaccharide structure, the results of our study are also similar to these studies. Therefore, we speculate that UV/H_2O_2 treatment induces the breakage of polysaccharide chains and the exposure of more groups and this treatment can reduce protein, polyphenol and pigment contents. Finaly, both effects may further increase the total carbohydrate of DMOLP-3 and modify its structure.

Table 1
Chemical compositions, particle size and zeta potential of MOLP and DMOLP-3.

Chemical composition	MOLP	DMOLP-3
Total carbohydrates(%)	46.5 ± 0.18[b]	50.7 ± 0.32[a]
Uronic Acid (%)	15.8 ± 0.45[b]	37.6 ± 1.02[a]
Protein (%)	15.3 ± 0.05 [a]	1.6 ± 0.05 [b]

3.3. Antioxidant properties of MOLP and DMOLP-3

Numerous diseases, including ageing, diabetes and cardiovascular disease are linked to oxidative stress and the excessive generation of Reactive oxygen species (ROS) (Zhang et al., 2023). Polysaccharides have been extensively studied as dietary antioxidants with the aim of improving health by neutralizing free radicals. (Liang et al., 2019). MOLP have been reported to have antioxidant activity (Dong et al., 2018). Thus, this study focused on the ABTS radical (Fig. 2A), DPPH radical (Fig. 2B) and hydroxyl radical (Fig. 2C) scavenging abilities of MOLP and DMOLP-3. The results clearly demonstrated the dose-dependent scavenging ability of both MOLP and DMOLP-3 toward these different types of free radicals. Among them, compared with MOLP, DMOLP-3 had a better scavenging effect, the antioxidant activity of DMOLP-3 was related to the change of its physical properties (Fig. 2D). These results indicated that DMOLP-3 may be developed as a natural antioxidant food material.

Polysaccharides have been studied as antioxidants that can improve overall health by neutralizing free radicals. Some studies have found that the antioxidant properties of polysaccharides have a significant correlation with their *M*w. Because low *M*w polysaccharides have better water solubility, they have larger surface area and more reduced hydroxyl groups. In addition, the degradation of chemical groups in polysaccharides increases the opportunity to interact with free radicals, not only by providing electrons to reduce free radicals to more stable forms, but also by reacting directly with free radicals to terminate the chain reaction. At the same time, the antioxidant activity of polysaccharides is also affected by their functional groups and chemical composition. Degradation may lead to the release of electrophilic groups, degraded polysaccharides may have more reducing hydroxyl groups, which can target and react with active free radicals. It is worth noting that the change of polysaccharide spatial configuration caused by partial degradation treatment may also affect its antioxidant activity. The treatment may significantly change the aggregation state, particle size and surface morphology of polysaccharide chain conformation by destroying covalent bonds, thereby enhancing its free radical scavenging ability (Chen et al., 2023). Although the polyphenol content decreased after UV / H_2O_2 treatment, the improvement of the antioxidant capacity of the degraded polysaccharide obtained after treatment was greater than the degree of polyphenol degradation. This may be due to factors such as the *M*w and monosaccharide composition of polysaccharides. Therefore, we next studied the *M*w, monosaccharide composition and appearance of DMOLP-3.

3.4. Effects of UV/H_2O_2 on M_W of MOLP and DMOLP-3

Fig. 3A-B shows the peak shapes of MOLP and DMOLP-3 are similar, indicating that the same polysaccharides was involved. Moreover, as the treatment time increases, the M_W of the MOLP decreased, the peak distribution of DMOLP-3 was relatively uniform. This observation may suggest that the treatment primarily targets longer chains and breaks them into smaller fragments, consequently altering the peak shape (Chen, You, et al., 2021; Gong et al., 2021). Notably, the MOLP contained two groups of polysaccharides with different M_W (3024 Da and 2142 Da, respectively) (Fig. 3A), whereas the DMOLP-3 polysaccharide had only one group of polysaccharides (2494 Da) (Fig. 3B). The decrease in the M_W of MOLP is primarily due to the breakage of glycosidic linkages caused by the presence of free radicals. It is widely recognised that the M_W of plant polysaccharides has an impact on their bioactivity (Li et al., 2013), excessively high M_W hinders the ability of these materials to penetrate cell membranes and exert pharmacological effects, whereas low M_W compromise the ability of these materials to form active polymer structures (Chen et al., 2023). In addition, the antioxidant properties of polysaccharides exhibit a substantial correlation with their M_W,

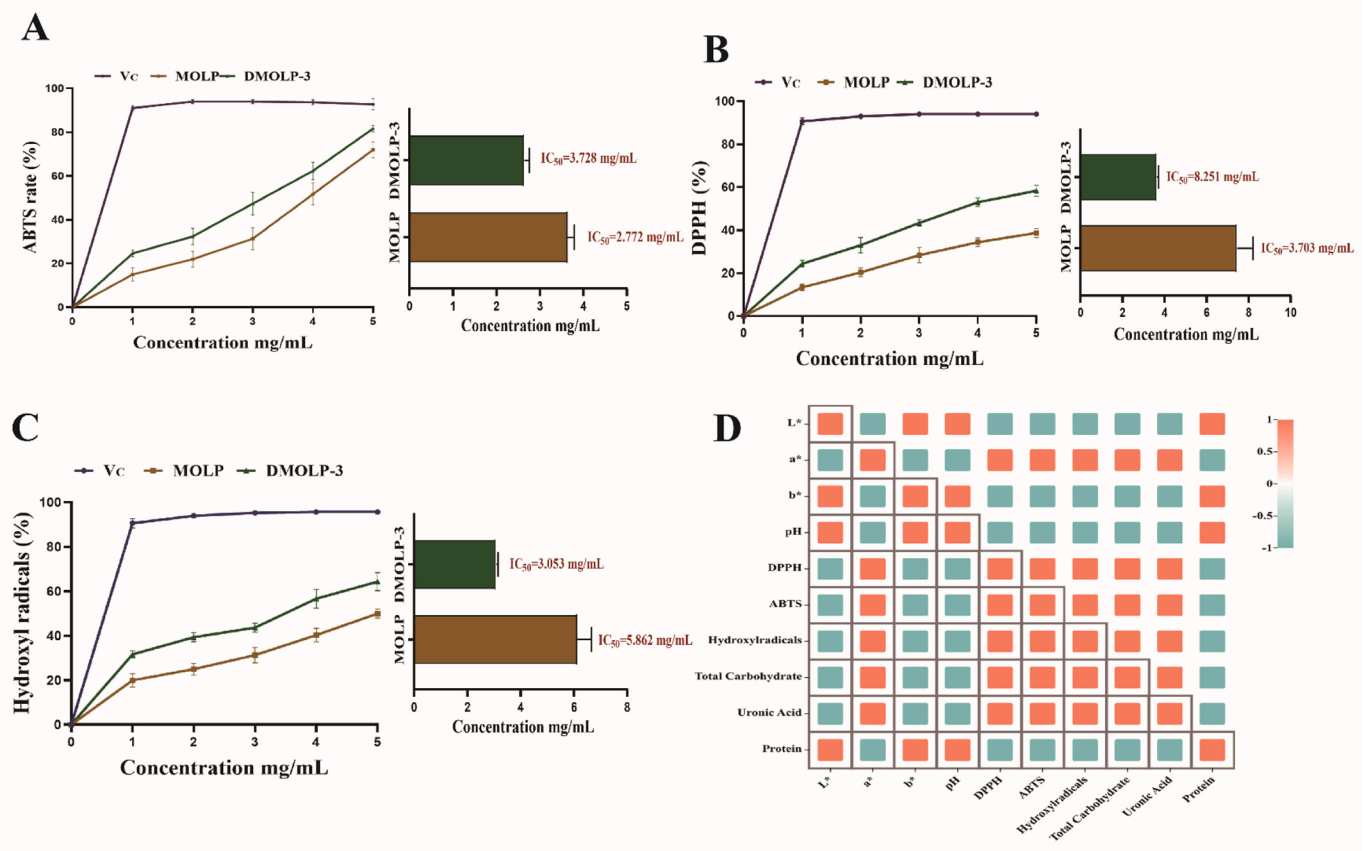

Fig. 2. The antioxidant properties of MOLP and DMOLP-3 (A). The ABTS scavenging percentage of MOLP and DMOLP-3; (B). The DPPH scavenging percentage of MOLP and DMOLP-3; (C). The Hydroxyl scavenging percentage of MOLP and DMOLP-3; (D). The relative between physicochemical properties scavenging percentage of MOLP and DMOLP-3.

and polysaccharides with lower M_W exhibit superior antioxidant activity. This can be explained that low-*M*w polysaccharides may have better water solubility, which increases their surface area and the number of hydroxyl groups. (Chen et al., 2023; Sun, Wang, Li, & Liu, 2014). Yan et al. (2021) found that the 2918 kDa polysaccharide from *coccidia cylindricum* polysaccharides has hardly any antioxidant activity, whereas the degraded polysaccharides (6.56 kDa) after H_2O_2/Vc/ ultrasound and H_2O_2/Fe^{2+}/ultrasound treatment showed better antioxidant activity. Therefore, degraded polysaccharides are known to possess enhanced biological activity, which can be attributed to changes in their physicochemical properties and structure.

3.5. Monosaccharide composition of MOLP and DMOLP-3

As shown in Fig. 3C and D, MOLP and DMOLP-3 were found to primarily consist of rhamnose, arabinose, galactose, glucose, xylose, mannose and galacturonic acid. The result indicate that the treatment did not alter the main types of monosaccharides present, which is consistent with the previous studies. (Chen et al., 2017). However, after treatment, there were slight changes in the molar ratio of the monosaccharides.

MOLP were composed of rhamnose (6.2%), arabinose (21.8%), galactose (44.8%), glucose (15.3%), xylose (2.2%), mannose (2.8%) and galacturonic acid (5.9%), with a molar ratio of 2.82:9.91:20.36:6.95:1.00:1.27:2.68. After UV/H_2O_2 treatment, DMOLP-3 was composed of rhamnose (4.5%), arabinose (16.7%), galactose (57.6%), glucose (11.6%), xylose (1.7%), mannose (1.3%), galacturonic acid (4.8%), and glucuronic acid (0.7%), with a molar ratio of 6.43:23.86:82.29:16.57:2.43:1.86:6.86:1.00. The results indicated a remarkable decrease in the molar ratio of arabinose to glucose within the MOLP, potentially suggesting the vulnerability of arabinose and glucose residues to free radicals (Chen, You, et al., 2021; Yao et al., 2022). Conversely, there was a notable increase in the molar ratio of galactose to glucuronic acid in DMOLP-3. This change was possibly attributed to the intricate composition of the polysaccharides and the non-discriminate assault of uncontrolled radicals (Chen, Sun-Waterhouse, et al., 2021; Zhu, Chen, Chang, Qiu, & You, 2023). Dong et al. (2018) discovered that MOLP can reduce the levels of Reactive oxygen species (ROS), Nitric oxide (NO), Interleukin-6 (IL-6) and Tumour necrosis factor-α (TNF-α) under specific galactose and uronic acid compositions. In summary, DMOLP-3, which contains more galactose and glucuronic acid with low M_W can be studied as antioxidant in the future.

3.6. FT-IR analysis of MOLP and DMOLP-3

The FT-IR spectra of MOLP and DMOLP-3 were compared and are shown in Fig. 3E, MOLP and DMOLP-3 displayed similar infrared characteristic peaks. The peak at 3300–3400 cm^{-1} was caused by the stretching vibration of O—H, which is the characteristic peak of polysaccharides (Cui et al., 2019). The peaks at 2924 cm^{-1} (MOLP) and 2922 cm^{-1} (DMOLP-3) were caused by C—H stretching vibrations (Yuan, Li, et al., 2020). The peak at 1603 cm^{-1} (MOLP) and 1606 cm^{-1} (DMOLP-3) may be attributed to the C═O asymmetric tensile vibration (Dong et al., 2018). There are absorption peaks at 1415 cm^{-1} (MOLP) and 1414 cm^{-1} (DMOLP-3) which may be attributed to the deformation vibration of the C—H bond and the incorporation of hydroxyls and carbonyls, respectively (Bissaro, Kommedal, Røhr, & Eijsink, 2020; Dong et al., 2018). The peak at approximately 1150–1010 cm^{-1} is due to the stretching vibration of the pyranose ring of the glycosyl residue (Wu

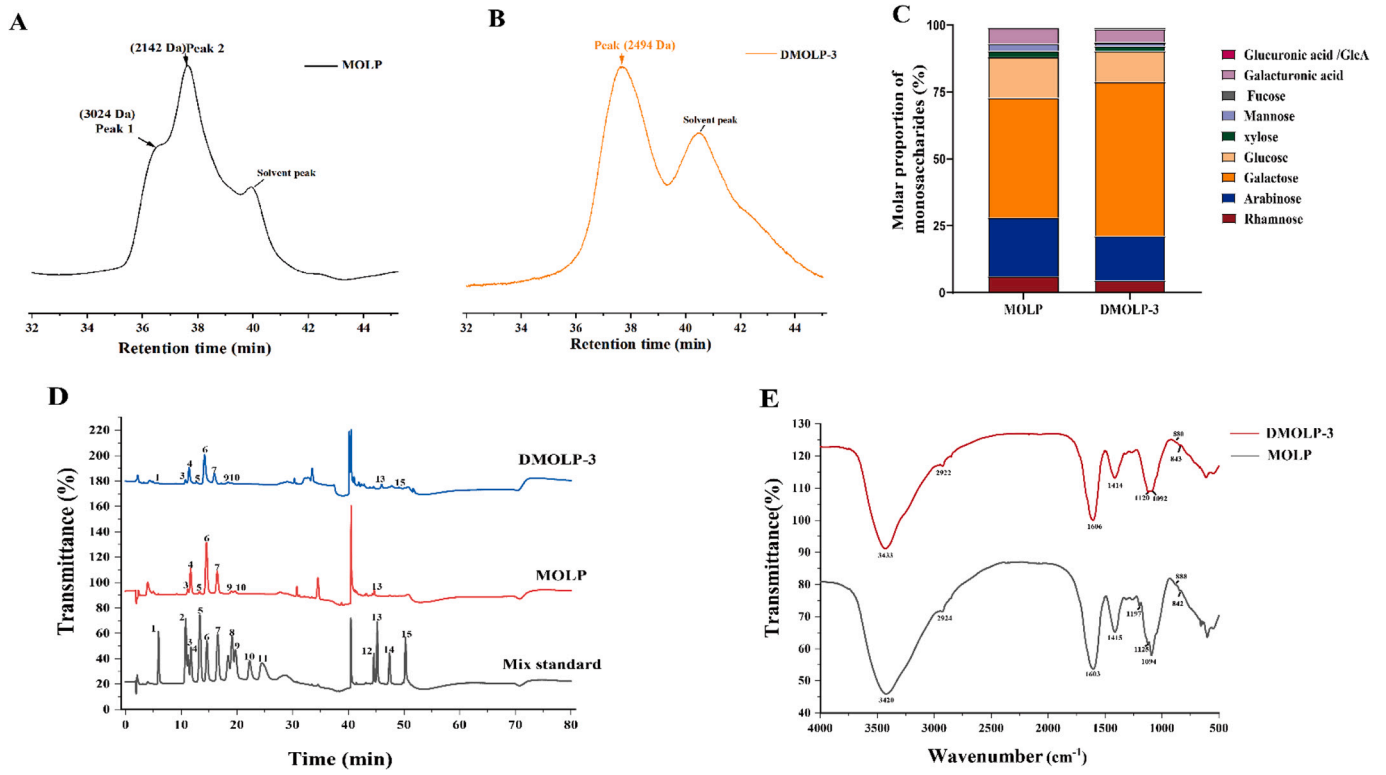

Fig. 3. The composition of MOLP and DMOLP-3 (A). Molecular weight of MOLP; (B). Molecular weight of DMOLP-3; (C). Monosaccharide composition of MOLP and DMOLP-3; (D). Ion chromatogram of the monosaccharide composition of MOLP and DMOLP-3; (E). FT-IR spectra of MOLP and DMOLP-3. In Fig. 3C: 1: Fuc, 2: GalN, 3: Rha, 4: Ara, 5: GlcN, 6: Gal, 7: Glc, 8: Xyl, 9: Man, 10: Fru, 11: Rib; 12: GalA, 13: GulA, 14: GlcA, 15: ManA.

et al., 2022). The absorption peaks in the range of 1000–1200 cm^{-1} were related to the C–O–H and C–O–C stretching spectra (Hu et al., 2023), indicating that MOLP and DMOLP-3 contained pyranose rings, but the peak shape of DMOLP-3 decreased, presumably due to UV/H_2O_2 degradation of polysaccharides that destroyed the sugar ring structure. In addition, the absorption peaks at approximately 888 cm^{-1} (MOLP) and 880 cm^{-1} (DMOLP-3) indicate the presence of α-glycosidic bonds (Li et al., 2020), and the absorption peaks at approximately 842 cm^{-1} (MOLP) and 843 cm^{-1} (DMOLP-3) indicate the presence of β-glycosidic bonds (Liu, Xue, Tong, Dong, & Wu, 2018). The results indicated that UV/H_2O_2 treatment did not alter the main functional groups present in the MOLP.

3.7. Congo red analysis of MOLP and DMOLP-3

Polysaccharides, which exhibit a triple helix conformation can form a complex with the Congo red. As a consequence of this complex formation, a shift in the maximum absorption wavelength occurs in comparison with that of the Congo red solution (Li, Guo, et al., 2020). However, as the concentration of NaOH increases, the complex arrangement disintegrates, causing a decrease in the maximum absorption wavelength of the solution (Dong et al., 2018). As shown in Fig. 4A, the highest wavelength at which Congo Red or polysaccharide absorption occurred did not redshift when the cells were subjected to various concentrations of NaOH solution, indicating that MOLP and DMOLP-3 may not contain a triple helix structure and suggesting that MOLP and DMOLP-3 may have disordered structures.

3.8. The particle size and zeta potential of MOLP and DMOLP-3

The stability of polysaccharides can be elucidated by considering the particle size and zeta potential of these compounds. Gong et al. (2021) indicated that enhancing the bioactivities of polysaccharides is achievable through particle size reduction. The particle size distribution, Polymer dispersity index (PDI) and zeta potential had important effects on the stability of the polysaccharides. A higher PDI indicates that the particle size distribution is more dispersed. Conversely, a smaller PDI indicates a more uniform distribution of polysaccharides, which also indicates greater stability.

The results shown in Fig. 4B clearly demonstrate the substantial reduction in the particle size of MOLP through UV/H_2O_2 treatment. The particle sizes of both MOLP and DMOLP-3 decreased gradually as the treatment time increased. Specifically, the average particle size decreased from 765.1 ± 2.01 nm (MOLP) to 479.3 ± 1.83 nm (DMOLP-3), indicating a notable reduction in particle size. This observation is consistent with the decrease in the M_W observed in Fig. 3A and B. As shown in Fig. 4C, the average PDI of the MOLP was 0.831 ± 1.05 nm, indicating that the particles were dispersed, the PDI of DMOLP-3 was 0.036 ± 1.26 nm, indicating that the polysaccharide distribution was relatively uniform and stable.

The zeta potential is used to characterise the surface charge properties of polysaccharides. The higher the absolute value of the zeta potential is, the easier it is for polysaccharides to disperse during dissolution (Sun et al., 2023). The average absolute zeta potential of DMOLP-3 (14.5 ± 1.84 mV) as considerably greater than that of the MOLP (8.79 ± 1.38 mV) (Fig. 4D). When the PDI decreased, the zeta potential increased, further confirming that UV/H_2O_2 treatment can increase the stability of DMOLP-3. These results suggest that DMOLP-3 may have better stability and solubility than MOLP.

3.9. SEM images of MOLP and DMOLP-3

The surface topographies of MOLP and DMOLP-3 were analysed using SEM. As shown in Fig. 4E and F, the MOLP had a rough surface morphology, the polysaccharides had a granular distribution, and the surface was thick and unevenly distributed. After UV/H_2O_2 treatment,

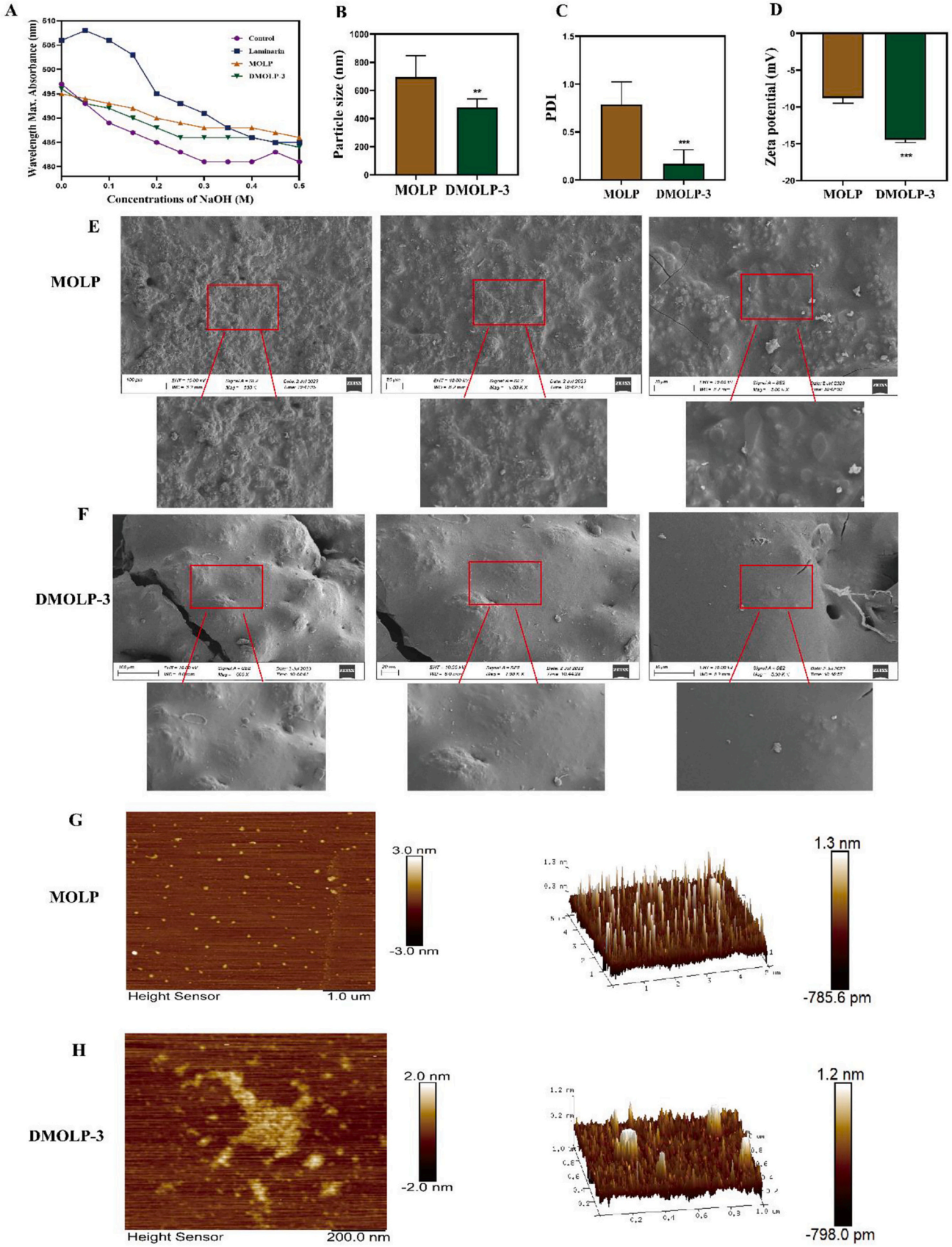

Fig. 4. The apparent appearance of MOLP and DMOLP-3 (A). Congo red analysis in the presence; (B). The particle sizes of MOLP and DMOLP-3; (C). The PDI of MOLP and DMOLP-3; (D). The zeta potential of MOLP and DMOLP-3; (*E*-F). SEM images of MOLP and DMOLP-3; (G-H). AFM planar and 3D images of MOLP and DMOLP-3. (For interpretation of the references to colour in this figure legend, the reader is referred to the web version of this article.)

the surface roughness and compactness of DMOLP-3 considerably decreased. Furthermore, a small amount of fragmentation was observed in DMOLP-3, possibly resulting from the hydrolysis of glycosidic linkages throughout the degradation procedure. At the same time, the surface of DMOLP-3 exhibits a smooth sheet shape. The morphological changes in MOLP and DMOLP-3 can be attributed to the attack of free radicals on the covalent bonds of polysaccharides, which reduces the degree of intermolecular cross-linking and is conducive to the depolymerisation of the polysaccharide backbone and substituents.

3.10. AFM measurements of MOLP and DMOLP-3

AFM was utilised to elucidate the morphology of polysaccharide samples because structures can be observed at the molecular level under near-natural conditions (Wang & Nie, 2019). As shown in Fig. 4G and H, MOLP and DMOLP-3 were irregular spherical clumps with uneven particle size distributions. The heights of the MOLP and DMOLP-3 were 1.3 ± 3.67 nm and 1.2 ± 2.49 nm, respectively. The protrusion height of MOLP was greater than that of DMOLP-3. In addition, the root mean square roughness and average roughness of the MOLP were measured to be 0.281 ± 0.16 nm and 0.154 ± 0.28 nm, respectively. However, for DMOLP-3, these values decreased to 0.220 ± 1.08 nm and 0.146 ± 0.95 nm, indicating that the surface of the MOLP was rougher than that of DMOLP-3. This observation could be attributed to the decrease in the M_W of DMOLP-3 compared with that of MOLP, as the M_W plays a substantial role in determining the surface roughness of the film. The results indicate that the surface roughness of the polysaccharide was notably influenced by UV/H_2O_2 treatment, which could be attributed to the impact of free radical attack, which disrupted the primary chain and reduced intermolecular hydrogen bonding. As a result, there was a decrease in both particles and agglomerates (Yao et al., 2022; Chen, Sun-Waterhouse, et al., 2021; Gong et al., 2021).

3.11. Methylation analysis of DMOLP-3

The monosaccharide linkage of DMOLP-3 was determined by methylation and GC–MS analysis. The GC–MS analysis results for DMOLP-3 are shown in Fig. 5A and Table 2 (Fig. S1 also showed the Ion current diagram of a single glycosidic bond) after comparison with the Complex Carbohydrate Research Center (CCRC) standard mass spectrometry database. The results showed that DMOLP-3 contained 10 glycosidic bonds. These glycosidic bonds mainly include Ara*f*-(1 → (37.3%), →5)-Ara*f*-(1 → (4.8%), Gal*p*-(1 → (6.0%), →3,5)-Ara*f*-(1 → (6.4%), →2,4)-Rha*p*-(1 → (5.2%), →4)-Gal*p*-(1 → (5.2%), →3)-Gal*p*-(1 → (5.2%), →6)-Gal*p*-(1 → (6.1%), →3,4)-Gal*p*-(1 → (13.1%) and →3,6)-Gal*p*-(1 → (3.2%). This finding is consistent with the monosaccharide composition results and confirmed that DMOLP-3 is composed mainly of galactose and arabinose.

Many studies have indicated that MOLP are rich in galactose and rhamnose (Yang, Lin, & Zhao, 2023). Li, Guo, et al. (2020) indicated that MOLP contain arabinose, glucose and galactose moieties and specific glycosidic bonds (1 → 3,6)-β-D-Gal*p*, (1 → 6)-β-D-Gal*p*, (1 → 5)-α-L-Ara*f* and T-α-L-Ara*f* can improve the immune response of RAW 264.7 cells and increase their pinocytosis capacity. Similarly, Cui et al. (2019) demonstrated that MOLPs with certain α-glycosidic bonds, such as α-Ara*f*, α-Gly, β-Gal*p*, α-Galp and β-Gly, exhibited improved immune capacity. Moreover, MOLP had the main effect. In addition, the main stems of MOLP exhibit a → 1)-β-D-Gal*p*-(3,4→) pattern with distinct branches at O-4 originating from →1)-β-D-Gal*p*-(4→,→1)-α-D-Gal*p*-(2 → Ara*f*-(1 → Gal*p*-(1 → branch chain, which enhances the iron-reducing

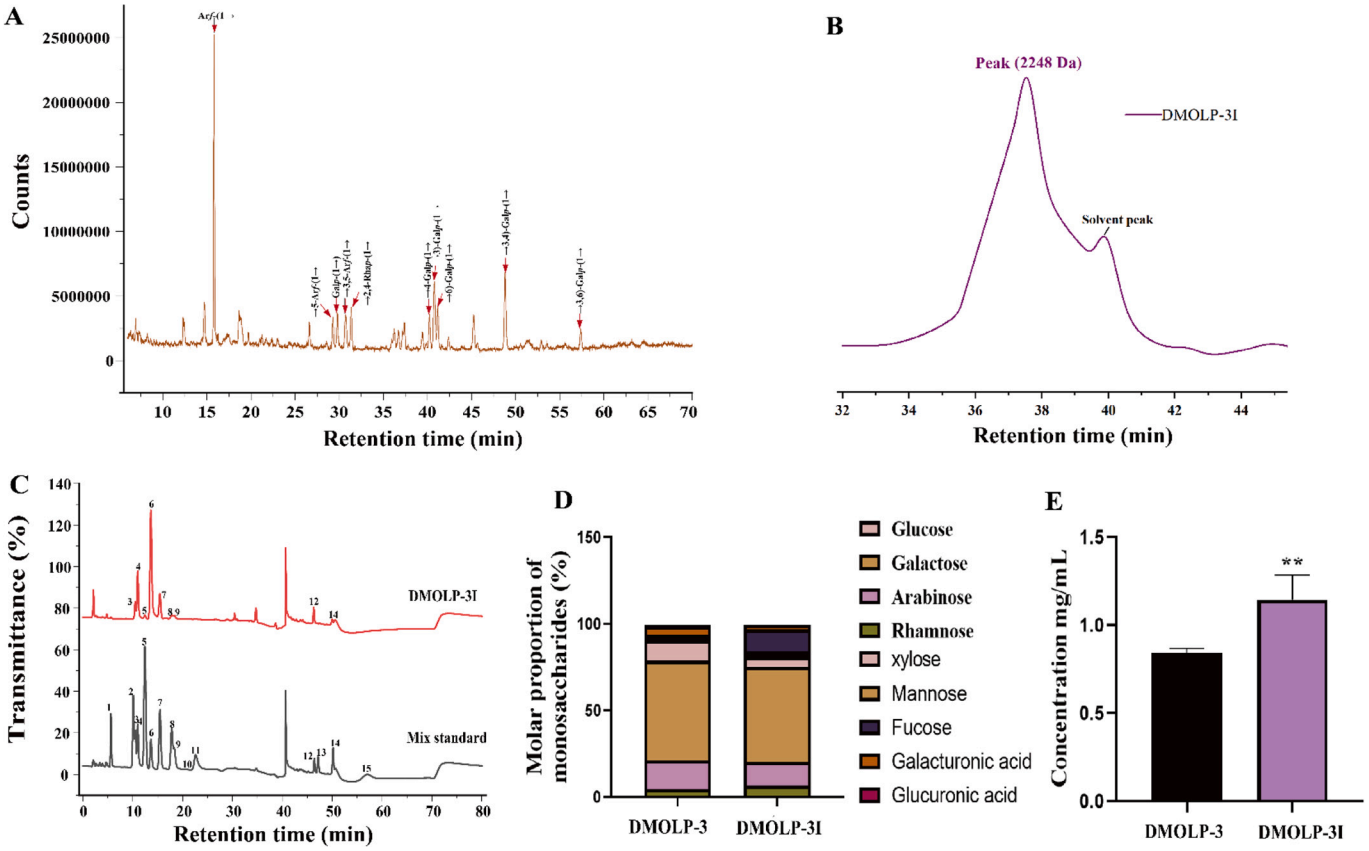

Fig. 5. The composition of DMOLP-3 and DMOLP-3I (A). GC–MS methylation analysis of DMOLP-3; (B) Molecular weight of DMOLP-3I; (C) Ion chromatogram of the monosaccharide composition of DMOLP-3I; (D) Monosaccharide composition of DMOLP-3 and DMOLP-3I; (E). The reducing sugar content of DMOLP-3 and DMOLP-3I. In Fig. 5C: 1: Fuc, 2: GalN, 3: Rha, 4: Ara, 5: GlcN, 6: Gal, 7: Glc, 8: Xyl, 9: Man, 10: Fru, 11: Rib; 12: GalA, 13: GulA, 14: GlcA, 15: ManA.

Table 2
Methylation analysis of DMOLP-3.

RT (min)	Methylated sugar	Mass fragments (*m/z*)	Molar ratio (%)	Type of linkage
15.813	2,3,5-Me_3-Ara*f*	43,71,87,101,117,129,145,161	37.3	Ara*f*-(1→
29.274	2,3-Me_2-Ara*f*	43,71,87,99,101,117,129,161,189	4.8	→5)-Ara*f*-(1→
29.791	2,3,4,6-Me_4-Gal*p*	43,71,87,101,117,129,143,161,205	6.0	Gal*p*-(1→
30.73	2-Me_1-Ara*f*	43,58,85,99,117,127,159,201	6.4	→3,5)-Ara*f*-(1→
31.369	3-Me_1-Rha*p*	43,87,101,117,129,143,159,189	5.2	→2,4)-Rha*p*-(1→
40.219	2,3,6-Me_3-Gal*p*	43,87,99,101,113,117,129,131,161,173,233	5.2	→4)-Gal*p*-(1→
40.777	2,4,6-Me_3-Gal*p*	43,87,99,101,117,129,161,173,233	12.6	→3)-Gal*p*-(1→
41.175	2,3,4-Me_3-Gal*p*	43,87,99,101,117,129,161,189,233	6.1	→6)-Gal*p*-(1→
48.793	2,6-Me_2-Gal*p*	43,87,99,117,129,149	13.1	→3,4)-Gal*p*-(1→
57.381	2,4-Me_2-Gal*p*	43,87,117,129,159,189,233	3.2	→3,6)-Gal*p*-(1→

RT: Retention time.

ability and subsequently enhances the scavenging potential of ABTS and DPPH (He et al., 2018). Our results are similar to these studies, suggesting that DMOLP-3 may have functional activity.

3.12. Characterisation of the physicochemical properties of DMOLP-3 during simulated gastrointestinal digestion

The digestion and absorption of nutrients is a complex process in the human digestive system. A low pH and enzyme activity in gastrointestinal fluid may lead to the degradation of polysaccharides (Li et al., 2024). As shown in the Fig. 5B, the M_w of the product (DMOLP-3I) after simulated gastrointestinal digestion was 2248 Da. The results indicated that the M_w of DMOLP-3 did not change considerably after simulated gastrointestinal digestion, which indicates that DMOLP-3 is only slightly degraded in simulated gastrointestinal. The composition of monosaccharides during fermentation can also be used to evaluate the digestion of polysaccharides in the body. As shown in the Fig. 5C and D, DMOLP-3I was composed of rhamnose (6.7%), arabinose (13.5%), galactose (55%), glucose (5.5%), xylose (1.3%), mannose (2.1%), galacturonic acid (12.8%), and glucuronic acid (2.8%), with a molar ratio of 5.15:10.38:42.31:4.23:1.00:1.62:9.85. The results indicated that the glucose was severely degraded, the galactose was slightly degraded, and the molar ratio of galacturonic acid to glucuronic acid increased, the main monosaccharides composition of DMOLP-3 did not significantly change during digestion.

The M_w of polysaccharides is reduced by cleavage of glycosidic bonds or depolymerisation of aggregates. Breakage of glycosidic polysaccharide bonds also leads to an increase in reducing sugar content (Hu et al., 2023). Therefore, the content of reducing sugars can reflect the degree of damage to glycosidic bonds by digestive enzymes. The results showed that the reducing sugar content of DMOLP-3 was 0.86 ± 0.23 mg/mL. After digestion, the reducing sugar content increased to 1.24 ± 0.31 mg/mL. The reducing sugar content also indicated that DMOLP-3 could be slight degraded by gastrointestinal digestive enzymes. The above results showed that during the simulated digestion, DMOLP-3 is only partially broken down in the gastrointestinal tract and the overall structure is relatively stable. In addition, it can be used as a prebiotic for intestinal microorganisms to produce probiotic metabolites such as SCFAs.

3.13. Effects of MOLP and DMOLP-3 on gut microbial diversity

To study the prebiotic properties of polysaccharides, researchers often use *in vitro* fermentation models. The use of *in vitro* fermentation models in polysaccharide research helps identify specific microorganisms involved in the degradation process and assess their impact on gut health (Dedhia, Marathe, & Singhal, 2022). The presence of polysaccharides in the intestine can promote microbial growth or generate advantageous metabolites, thereby modulating the human circulatory system and promoting overall well-being (Duque et al., 2021). MOLP regulate gut microbial health (Li et al., 2021; Wang et al., 2019). Therefore, we next used an *in vitro* faecal fermentation model to further study the prebiotic properties of DMOLP-3.

A total of 844,928 valuable sequences were obtained in this study. The dilution curve based on the Chao1 and Sobs indices accurately represented a substantial amount of microbial diversity information in this particular sample (Fig. 6A, B). According to the classification curve, the number of samples was sufficient, and the species distribution within the community was relatively equal. Furthermore, the analysis conducted using Bray–Curtis dissimilarity revealed that MOLP has a significant difference trend relative to the principal coordinate PCoA (PC1: 95.94%; PC2: 1.91%) compared with DMOLP-3 (Fig. 6C). This observation strongly suggested that the composition of gut microorganisms during DMOLP-3 fermentation is noticeably different from that MOLP fermentation. In addition, compared with MOLP group, the Sobs index in the DMOLP-3 group was notably lower. This outcome could be attributed to the fermentation process associated with DMOLP-3 prompting an increase in certain gut microorganisms while concurrently causing a decrease in community diversity (Fig. 6D).

3.14. Effects of MOLP and DMOLP-3 on the overall structure of the microbial community

As shown in Fig. 6E and F, the dominant bacteria identified in the MOLP and DMOLP-3 groups were Firmicutes, Bacteroidota, Proteobacteria and Actinobacteriota, which are normal components of the human gut microbiota. In addition, after 24 h of *in vitro* fermentation, the composition of the DMOLP-3 group was different from that of the MOLP group. Compared with those in MOLP group, the relative abundances of Firmicutes, Bacteroidetes, and Actinobacteria in DMOLP-3group increased, while the relative abundance of Proteobacteria decreased. The Firmicutes can cause indigestion of the gut, while the Proteobacteria is regarded as a potential indicator of both intestinal inflammation and intestinal cancer (Wu et al., 2022). Low M_w polysaccharides are easily absorbed by the body and also showed a positive effect on regulating gut microbes (Chen et al., 2023). Moreover, Firmicutes can generate SCFAs through the fermentation of carbohydrates (Tawfick, Xie, Zhao, Shao, & Farag, 2022). We also evaluated different microorganisms at the genus level (Fig. 6G, H). The abundance of *Bacteroides* and *Bifidobacterium* was higher in the DMOLP-3 group than in the MOLP group. *Bacteroides* and *Bifidobacterium* are well-known probiotics that have been shown to produce SCFAs, which are effective at reducing gut inflammation (Wang et al., 2019). In addition, the abundance of *Escherichia–Shigella* decreased in the DMOLP-3 group, research indicated that *Escherichia–Shigella* caused severe gut disease by producing toxins (Wu et al., 2021). Both of these results suggest that DMOLP-3 may have certain prebiotic advantages over MOLP in regulating gut microbes.

3.15. LEfSe analyses of changes in key taxonomic species

We obtained different levels of dominant bacteria in each group by LEfSe and LDA analyses (Fig. 7A, B). Fig. 7C shown that compared with

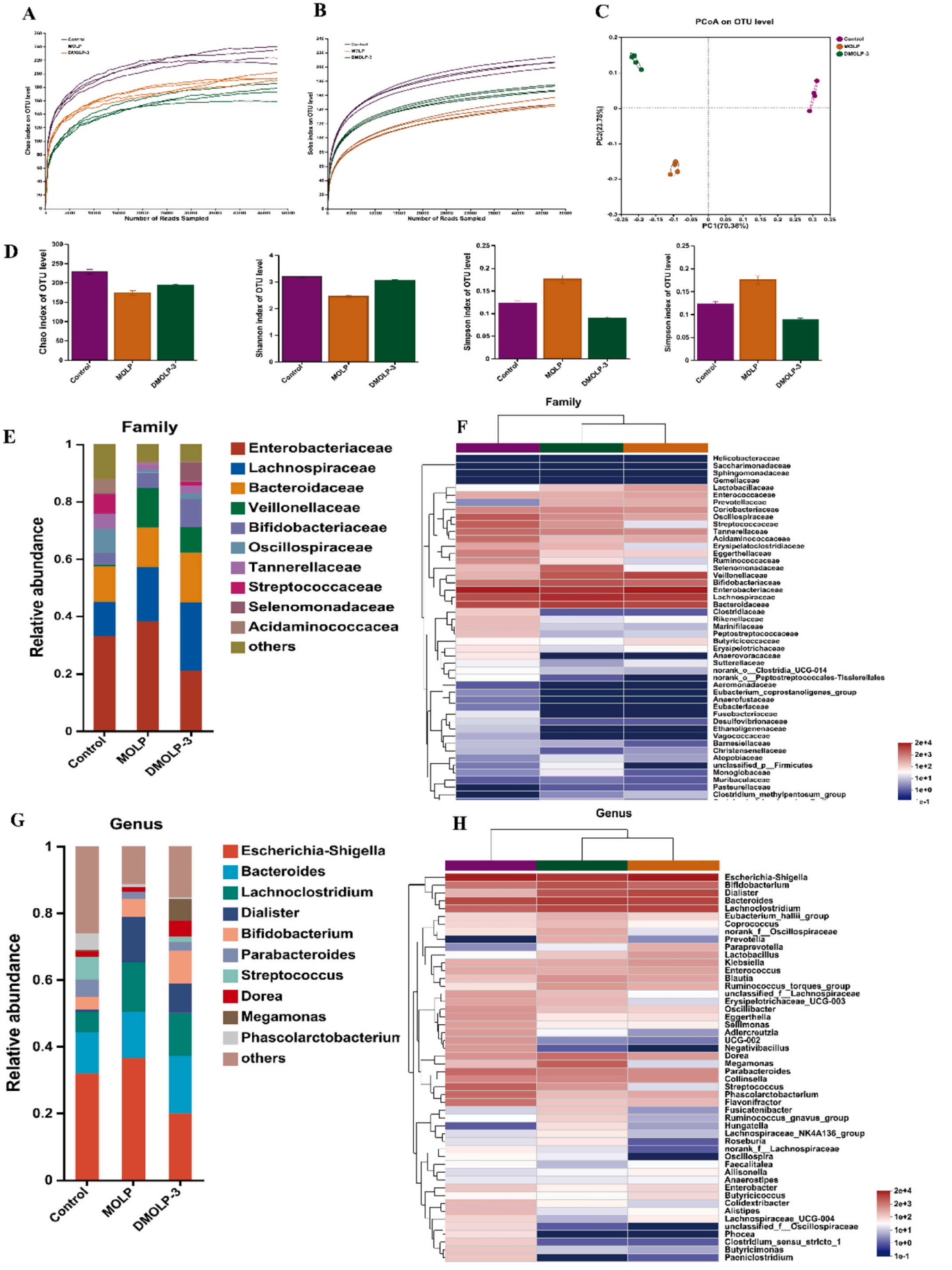

(caption on next page)

Fig. 6. The human microbiota community was affected in the MOLP and DMOLP-3 groups after 24 h fermentation. (A-B) Chao1 and Sobs dilution curve indices of MOLP and DMOLP-3; (C) PCoA of MOLP and DMOLP-3; (D). Chao1, Shannon, and simpson indices of MOLP and DMOLP-3; (E). The relative abundance of bacterial community at the family; (F) The relative abundance of bacterial community thermography at the family level; (G). The relative abundance of bacterial community at the genus level; (H) The relative abundance of bacterial community thermography at the genus level.

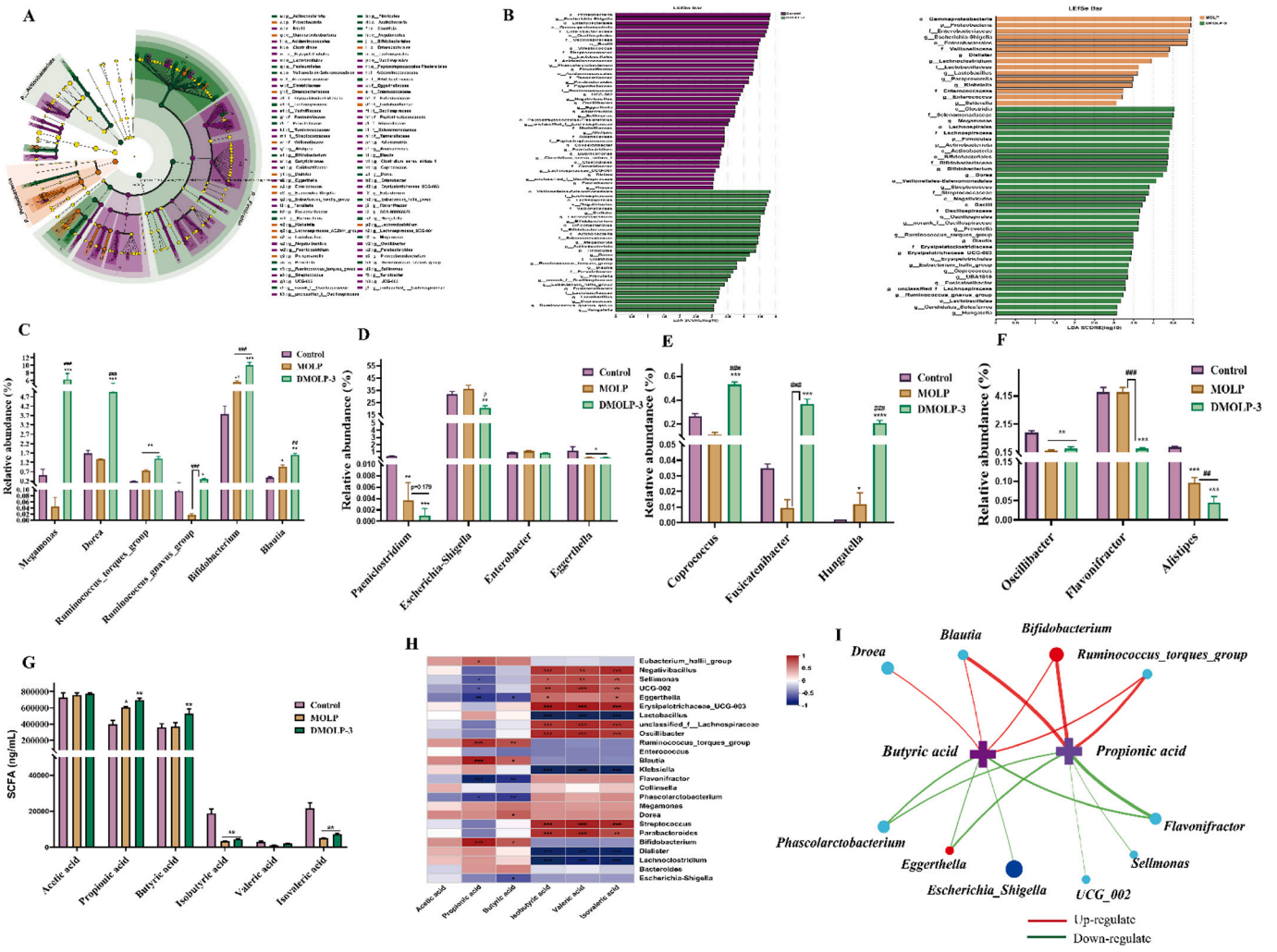

Fig. 7. The differences in gut microbes were compared based on LEfSe and LDA scores. (A). LEfSe analysis of MOLP and DMOLP-3 at the OTUs level; (B). LDA scores among MOLP and DMOLP-3 at the OTU level; (C). Positively regulated microorganisms among MOLP and DMOLP-3 at the OTUs level; (D). Negatively regulate microorganisms among MOLP and DMOLP-3 at OTUs level; (E). Positively regulated of nerve microorganisms among the MOLP and DMOLP-3 strains at the OTU level; (F). Negatively regulate nerve-microorganisms among MOLP and DMOLP-3 at OTUs level; (G). The concentrations of SCFAs among MOLP and DMOLP-3; (H—I). Spearman Correlation analysis between genus level microorganism and SCFAs among MOLP and DMOLP-3. All the data are expressed as the means ± SEM from three independent experiments, and significance was determined using an unpaired *t*-test; $*p < 0.05$, $**p < 0.01$, and $***p < 0.001$ *vs.* the control; $\#p < 0.05$, $\#\#p < 0.01$, and $\#\#\#p < 0.001$ *vs.* the MOLP group.

control group, the levels of intestinal probiotics related to SCFAs synthesis (such as *Megamonas*, *Dorea*, *Ruminococcus_torques_group*, *Ruminococcus_gnavus_group*, *Bifidobacteria*, and *Blautia*) were higher in the MOLP and DMOLLP-3 groups. This phenomenon indicated an increased abundance of these beneficial bacteria in the MOLP and DMOLLP-3 groups. Interestingly, compared with MOLP group, the levels in the DMOLP-3 group were substantially higher, indicating that DMOLP-3 increases the relative abundance of intestinal probiotics, thereby promoting human intestinal health. Many studies have demonstrated the ability of these gastrointestinal microorganisms to ferment and metabolise carbohydrates to produce various forms of SCFAs. Additionally, these probiotics have been shown to support the maintenance and stabilisation of the intestinal mucosal barrier while modulating the immune function of the gut (Wu et al., 2020; Wu et al., 2022). Some Research indicated that *Ruminococcus_torques_group* and *Ruminococcus_gnavus_group* can inhibit the activation of the Nuclear factor kappa-B (NF-κB) pathway and exert intestinal anti-inflammatory effects (Colin et al., 2023). *Bifidobacterium* species not only can treat intestinal infections but also prevent endotoxin from damaging the liver through blood by inhibiting the number of harmful bacteria that produce endotoxin (Perez-Burillo et al., 2021). *Blautia* can activate G protein-coupled receptors, namely, GPR41 and GPR43, resulting in the inhibition of insulin signalling and fat accumulation in adipocytes (Liu et al., 2021).

In contrast, compared with those in the control group, the abundance of *Paeniclostridium*, *Escherichia–Shigella*, *Enterobacter* and *Eggerthella* in the MOLP and DMOLP-3 fermentation groups decreased (Fig. 7D). These harmful bacteria can cause intestinal tissue necrosis and induce serious diseases, such as intestinal toxaemia and toxic shock. Among these bacteria, *Escherichia–Shigella* and *Enterobacter* have been shown to cause

serious diseases by producing toxins, and a high abundance of *Eggerthella* can aggravate obesity-related metabolic syndrome (Tawfick et al., 2022; Wang et al., 2019).

In addition, our study demonstrated that the fermentation of MOLP and DMOLP-3 has the potential to promote the proliferation of beneficial microorganisms related to neurocognitive functions, such as *Lachnospiraceae* (Fig. 7E). In the DMOLP-3 group, there was a substantial increase in the relative abundance of *Coprococcus*, *Fusicatenibacter* and *Hungatella* compared with that in the other groups. These gut microbes can play a positive neuroprotective role by fermenting carbohydrates and regulating brain–gut axis microorganisms. These protective effects mainly include the prevention of Parkinson's disease and cerebral aneurysms; the gut microbes that can regulate human emotions (related to depression) showed a substantial negative correlation (Valles-Colomer et al., 2019).

More importantly, we also evaluated changes in several harmful bacteria associated with intestinal nerves (Fig. 7F). The results showed that the abundances of *Oscillibacter*, *Flavonifractor* and *Alistipes* decreased in the MOLP and DMOLP-3 groups, especially in the DMOLP-3 group. The se harmful bacteria are inversely related to good neurological status, and higher levels of these bacteria may lead to stroke, temporary brain damage, or depression (Liu et al., 2021).

These results may indicate that DMOLP-3 plays a more beneficial role in regulating gut microbe communities than MOLP.

3.16. Changes in SCFAs levels after MOLP and DMOLP-3 fermentation

Gut microbes convert indigestible carbohydrates into SCFAs, which are critical for maintaining gut function and human health. SCFAs such as acetate, propionate, and butyrate have been shown to have a variety of positive effects on gut health. For instance, acetate has been found to regulate gut motility and improve digestive function (Wang et al., 2019). Propionate has been associated with reducing inflammation in the gut and preventing colitis (Tawfick et al., 2022), and butyrate has been shown to play a crucial role in promoting the growth and differentiation of intestinal cells (Wang et al., 2019). After 24 h of fermentation, the main fermentation products of the MOLP and DMOLP-3 groups were significantly different from those of the control group. Interestingly, the fermentation of DMOLP-3 had a more substantial impact on the production of SCFAs than did the fermentation of MOLP. Notably, acetic acid, propionic acid and butyric acid were the predominant substances generated during this process (Fig. 7G). Moreover, butyric acid production was greater in the MOLP group and DMOLP-3 group. Studies have shown that propionate metabolism serves the gluconeogenic pathway and inhibits cholesterol synthesis. Additionally, the presence of butyrate provides a valuable source of energy to intestinal epithelial cells, which in turn plays an important role in preventing the onset of colon disease, reducing intestinal inflammation, and improving the overall function of the intestinal barrier (Perez-Burillo et al., 2021).

In summary, gut microbes can utilise MOLP and DMOLP-3 to produce SCFAs. The DMOLP-3 group produced greater amounts of propionic acid and butyric acid than did the MOLP group. This result suggested that DMOLP-3 can be decomposed by intestinal microorganisms and ultimately contribute to the prebiotic effect of these bacteria.

3.17. Correlations between SCFAs and gut microbes produced through MOLP and DMOLP-3 fermentation

Based on our results, we evaluated the relationship between SCFAs production and intestinal microbial growth during fermentation with MOLP or DMOLP-3. In the present study, we investigated the possible associations between SCFAs and intestinal microbial growth during fermentation.

The results indicated that there was a substantial positive correlation between the abundance of gene groups (*Eubacterium_hallii_group*, *Ruminococcus_torques_group*, *Blautia*, and *Bifidobacterium*) and the concentrations of propionic acid and butyric acid. In addition, the abundance of *Dorea* was strongly positively correlated with the concentration of butyric acid. These results suggest a potential relationship between these bacterial groups and the production of propionic acid and butyric acid. In contrast, the abundances of *Sellimonas*, *Flavonifractor*, *UCG-002*, *Eggerthella* and *Phascolarctobacteriu*m were negatively correlated with propionate concentration. These results indicate that the abundance of these bacteria decreases as the propionate concentration increases. There was a negative correlation between the concentration of butyric acid and the abundance of *Eggerthella*, *Flavonifractor*, *Phascolarctobacterium* and *Escherichia–Shigella* in the DMOLP-3 group (Fig. 7H, I).

Based on our results, it can be inferred that DMOLP-3 holds promising potential as a prebiotic raw material in the future food industry. The results of our study suggest that DMOLP-3 is suitable for use in the production of prebiotic foods. Therefore, further investigations and additional research are needed to fully explore the potential and benefits of DMOLP-3 in the food industry.

4. Conclusions

This study focused on evaluating the composition, antioxidant activity and prebiotic properties of polysaccharides from *Moringa oleifera* Lam. leaves that were treated with UV/H_2O_2, UV/H_2O_2 treatment significantly reduced the colour, M_w and particle size of the MOLPs and changed their surface morphology. Compared to MOLP, DMOLP-3 has an increased molar ratio of galactose to glucuronic acid, thereby improving its antioxidant activity. Moreover, DMOLP-3 contained 10 glycosidic bonds. These glycosidic bonds mainly include Ara*f*-(1 → (37.3%), →5)-Ara*f*-(1 → (4.8%), Gal*p*-(1 → (6.0%), →3,5)-Ara*f*-(1 → (6.4%), →2,4)-Rha*p*-(1 → (5.2%), →4)-Gal*p*-(1 → (5.2%), →3)-Gal*p*-(1 → (5.2%), →6)-Gal*p*-(1→, (6.1%), →3,4)-Gal*p*-(1 → (13.1%) and →3,6)-Gal*p*-(1 → (3.2%). In addition, *in vitro* simulated digestion experiments showed that DMOLP-3 was only partially degraded during gastrointestinal digestion, indicating that DMOLP-3 can be utilised by gut microorganisms. Therefore, we used an *in vitro* human faecal model to ferment these two polysaccharides. These results indicate that DMOLP-3 has better prebiotic effects than MOLP in the gut. Overall, the results indicated that DMOLP-3 has a significant impact on gut health by increasing the abundance of beneficial bacteria and reducing the abundance of harmful bacteria. In addition, DMOLP-3 can promote the production of SCFAs by intestinal microorganisms. Therefore, through this study, DMOLP-3 may be a new prebiotic dietary raw material for regulating intestinal health by improving the intestinal microbial environment.

Funding

This study was supported by the "Cassava Industrial Technology System of China" (CARS-11-YNTY), the "Yunnan Province-City Integration Project" (202302 AN360002), the "Yunnan Province-City Integration Project" (202302AN360002), and the "Yunnan Innovation Team of Food and Drug Homologous Functional Food" (202305AS350025).

CRediT authorship contribution statement

Min Yang: Writing – original draft, Data curation. **Liang Tao:** Writing – original draft, Formal analysis, Data curation. **Zi-Lin Wang:** Formal analysis, Data curation. **Ling-Fei Li:** Writing – review & editing. **Cun-Chao Zhao:** Formal analysis, Data curation. **Chong-Ying Shi:** Writing – review & editing, Supervision. **Jun Sheng:** Project administration, Conceptualization. **Yang Tian:** Writing – review & editing, Project administration, Funding acquisition.

Declaration of competing interest

The authors declare that there are no conflicts of interest.

Data availability

No data was used for the research described in the article.

Acknowledgements

We appreciate eceshi (www.eceshi.com) for the FTIR, SEM and AFM analyses.

Appendix A. Supplementary data

Supplementary data to this article can be found online at https://doi.org/10.1016/j.fochx.2024.101272.

References

Abou Zeid, A. H., Aboutabl, E. A., Sleem, A. A., & El-Rafie, H. M. (2014). Water soluble polysaccharides extracted from Pterocladia capillacea and Dictyopteris membranacea and their biological activities. *Carbohydrate Polymers, 113*, 62–66. https://doi.org/10.1016/j.carbpol.2014.06.004

Bissaro, B., Kommedal, E., Røhr, Å. K., & Eijsink, V. G. H. (2020). Controlled depolymerization of cellulose by light-driven lytic polysaccharide oxygenases. *Nature Communications, 11*, 890. https://doi.org/10.1038/s41467-020-14744-9

Bitter, T., & Muir, H. M. (1962). A modified uronic acid carbazole reaction. *Analytical Biochemistry, 4*(4), 330–334. https://doi.org/10.1016/0003-2697(62)90095-7

Chen, C., Zhang, B., Huang, Q., Fu, X., & Liu, R. H. (2017). Microwave-assisted extraction of polysaccharides from Moringa oleifera Lam. leaves: Characterization and hypoglycemic activity. *Industrial Crops and Products, 100*, 1–11. https://doi.org/10.1016/j.indcrop.2017.01.042

Chen, S., Liu, H., Yang, X., Li, L., Qi, B., Hu, X., … Pan, C. (2020). Degradation of sulphated polysaccharides from *Grateloupia livida* and antioxidant activity of the degraded components. *International Journal of Biological Macromolecules, 156*, 660–668. https://doi.org/10.1016/j.ijbiomac.2020.04.108

Chen, S. K., Wang, X., Guo, Y. Q., Song, X. X., Yin, J. Y., & Nie, S. P. (2023). Exploring the partial degradation of polysaccharides: Structure, mechanism, bioactivities, and perspectives. *Comprehensive Reviews in Food Science and Food Safety, 22*(6), 4831–4870. https://doi.org/10.1111/1541-4337.13244

Chen, X. Y., Sun-Waterhouse, D. X., Yao, W. Z., Li, X., Zhao, M. M., & You, L. J. (2021). Free radical-mediated degradation of polysaccharides: Mechanism of free radical formation and degradation, influence factors and product properties. *Food Chemistry, 365*, Article 130524. https://doi.org/10.1016/j.foodchem.2021.130524

Chen, X. Y., You, L. J., Ma, Y. X., Zhao, Z. Z., & Kulikouskay, V. (2021). Influence of UV/H_2O_2 treatment on polysaccharides from *Sargassum fusiforme*: Physicochemical properties and RAW 264.7 cells responses. *Food and Chemical Toxicology, 153*, Article 112246. https://doi.org/10.1016/j.fct.2021.112246

Colin, B., Ekaterina, V. K., Lisa, S., Cara, M. H., Biancav, A. N., & Colin, H. (2023). Temperate bacteriophages infecting the mucin-degrading bacterium *Ruminococcus* gnavus from the human gut. *Gut Microbes, 15*(1), 2194794. https://doi.org/10.1080/19490976.2023.2194794

Cui, C., Chen, S., Wang, X., Yuan, G., Jiang, F., Chen, X., & Wang, L. (2019). Characterization of Moringa oleifera roots polysaccharide MRP-1 with anti-inflammatory effect. *International Journal of Biological Macromolecules, 132*, 844–851. https://doi.org/10.1016/j.ijbiomac.2019.03.210

Dedhia, N., Marathe, S. J., & Singhal, R. S. (2022). Food polysaccharides: A review on emerging microbial sources, bioactivities, nanoformulations and safety considerations. *Carbohydrate Polymers, 287*, Article 119355. https://doi.org/10.1016/j.carbpol.2022.119355

Dengta, G. J., Banshtu, T. J., Verma, C. S., Gautam, N. H., & Sharma, P. (2023). Effect of total phenol on the control of leafminer (Phytomyza horticola) infestation in pea plants. *Natural Product Research, 16*, 1–7. https://doi.org/10.1080/14786419.2023.2282115

Dong, Z., Li, C., Huang, Q., Zhang, B., Fu, X., & Liu, R. H. (2018). Characterization of a novel polysaccharide from the leaves of *Moringa oleifera* and its immunostimulatory activity. *Journal of Functional Foods, 49*, 391–400. https://doi.org/10.1016/j.jff.2018.09.002

Dou, Z., Chen, C., & Fu, X. (2019). Bioaccessibility, antioxidant activity and modulation effect on gut microbiota of bioactive compounds from *Moringa oleifera* Lam. leaves during digestion and fermentation in vitro. *Food & Function, 10*(8), 5070–5079. https://doi.org/10.1039/c9fo00793h

Duque, A., Demarqui, F. M., Santoni, M. M., Zanelli, C. F., Adorno, M. A. T., Milenkovic, D., … Sivieri, K. (2021). Effect of probiotic, prebiotic, and synbiotic on the gut microbiota of autistic children using an *in vitro* gut microbiome model. *Food Research International, 149*, Article 110657. https://doi.org/10.1016/j.foodres.2021.110657

Feng, Y. Q., Qiu, Y. J., Duan, Y. Q., He, Y. Q., Xiang, H., Sun, W. X., & Ma, H. L. (2022). Characterization, antioxidant, antineoplastic and immune activities of selenium modified Sagittaria sagittifolia L. polysaccharides. *Food Research International, 153*, Article 110913. https://doi.org/10.1016/j.foodres.2021.110913

Gao, X., Xie, Q., Liu, L., Kong, P., Sheng, J., & Xiang, H. (2017). Metabolic adaptation to the aqueous leaf extract of Moringa oleifera Lam.-supplemented diet is related to the modulation of gut microbiota in mice. *Applied Microbiology and Biotechnology, 101*(12), 5115–5130. https://doi.org/10.1007/s00253-017-8233-5

Gong, Y. F., Ma, Y. X., Cheung, P. C. K., You, L. J., Liao, L., Pedisi, S., & Kulikouskay, V. (2021). Structural characteristics and anti-inflammatory activity of UV/H_2O_2-treated algal sulfated polysaccharide from *Gracilaria lemaneiformis*. *Food and Chemical Toxicology, 153*, Article 112246. https://doi.org/10.1016/j.fct.2021.112246

He, T. B., Huang, Y. P., Huang, Y., Wang, X. J., Hu, J. M., & Sheng, J. (2018). Structural elucidation and antioxidant activity of an arabinogalactan from the leaves of Moringa oleifera. *International Journal of Biological Macromolecules, 112*, 126–133. https://doi.org/10.1016/j.ijbiomac.2018.01.110

Hou, Y., Wang, J., Jin, W. H., Zhang, H., & Zhang, Q. B. (2012). Degradation of Laminaria japonica fucoidan by hydrogen peroxide and antioxidant activities of the degradation products of different molecular weights. *Carbohydrate Polymers, 87*, 153–159. https://doi.org/10.1016/j.carbpol.2011.07.031

Hu, W., Di, Q., Liang, T., Zhou, N., Chen, H. X., Zeng, Z. H., … Shaker, M. (2023). Effects of in vitro simulated digestion and fecal fermentation of polysaccharides from straw mushroom (Volvariella volvacea) on its physicochemical properties and human gut microbiota. *International Journal of Biological Macromolecules, 239*, Article 124188. https://doi.org/10.1016/j.ijbiomac.2023.124188

Hui, H. C., Wang, Z. Y., Zhao, X. R., Xu, L., Yin, L. H., Wang, F. F., … Peng, J. Y. (2023). Gut microbiome-based thiamine metabolism contributes to the protective effect of one acidic polysaccharide from Selaginella uncinata (Desv.) Spring against inflammatory bowel disease. *Journal of Pharmaceutical Analysis*. https://doi.org/10.1016/j.jpha.2023.08.003. in press.

Li, B., Liu, S., Xing, R., Li, K., Li, R., Qin, Y., … Li, P. (2013). Degradation of sulfated polysaccharides from *Enteromorpha prolifera* and their antioxidant activities. *Carbohydrate Polymers, 92*(2), 1991–1996. https://doi.org/10.1016/j.carbpol.2012.11.088

Li, C., Dong, Z., Zhang, B., Huang, Q., Liu, G., & Fu, X. (2020). Structural characterization and immune enhancement activity of a novel polysaccharide from *Moringa oleifera* leaves. *Carbohydrate Polymers, 234*, Article 115897. https://doi.org/10.1016/j.carbpol.2020.115897

Li, C., Zhou, S., Fu, X., Huang, Q., & Chen, Q. (2021). In vitro digestibility and prebiotic activities of a bioactive polysaccharide from Moringa oleifera leaves. *J Food Biochem, 45*(11), Article e13944. https://doi.org/10.1111/jfbc.13944

Li, J. T., Ye, F. Y., Zhou, Y., Lei, L., Chen, J., Li, S., & Zhao, G. H. (2024). Tailoring the composition, antioxidant activity, and prebiotic potential of apple peel by aspergillus oryzae fermentation. *Food Chemistry: X, 21*, Article 101134. https://doi.org/10.1016/j.fochx.2024.101134

Li, X. J., Guo, R., Wu, X. J., Liu, X., Ai, L. Z., Sheng, Y., … Wu, Y. (2020). Dynamic digestion of tamarind seed polysaccharide: Indigestibility in gastrointestinal simulations and gut microbiota changes *in vitro*. *Carbohydrate Polymers, 239*, Article 116194. https://doi.org/10.1016/j.carbpol.2020.116194

Liang, X., Gao, Y., Pan, Y., Zou, Y., He, M., He, C., … Lv, C. (2019). Purification, chemical characterization and antioxidant activities of polysaccharides isolated from Mycena dendrobii. *Carbohydrate Polymers, 203*, 45–51. https://doi.org/10.1016/j.carbpol.2018.09.046

Liu, P., Xue, J., Tong, S., Dong, W., & Wu, P. (2018). Structure characterization and hypoglycaemic activities of two polysaccharides from Inonotus obliquus. *Molecules, 23*(8), 1948. https://doi.org/10.3390/molecules23081948

Liu, X., Mao, B., Gu, J., Wu, J., Cui, S., Wang, G., … Chen, W. (2021). Blautia-a new functional genus with potential probiotic properties? *Gut Microbes, 13*(1), 1–21. https://doi.org/10.1080/19490976.2021.1875796

Ma, C. L., Bai, J. W., Shao, C. T., Liu, J. W., Zhang, Y., Li, X. Q., … Wang, L. B. (2021). Degradation of blue honeysuckle polysaccharides, structural characteristics and antiglycation and hypoglycemic activities of degraded products. *Food Research International, 143*, Article 110281. https://doi.org/10.1016/j.foodres.2021.110281

Ma, Z. F., Ahmad, J., Zhang, H., Khan, I., & Muhammad, S. (2020). Evaluation of phytochemical and medicinal properties of Moringa (Moringa oleifera) as a potential functional food. *South African Journal of Botany, 129*, 40–46. https://doi.org/10.1016/j.sajb.2018.12.002

Ma, X., Dong, L., He, Y., Chen, S. W. (2022). Effects of ultrasound-assisted H_2O_2 on the solubilization and antioxidant activity of yeast β-glucan. *Ultrasonics Sonochemistry* 90, 106210. doi:10.1016/j.ultsonch.2022.106210.

Minekus, M., Alminger, M., Alvito, P., Ballance, S., Bohn, T., & Bourlieu, C. (2014). A standardised static in vitro digestion method suitable for food – An international consensus. *Food & Function, 5*(6), 1113–1124. https://doi.org/10.1039/c3fo60702j

Perez-Burillo, S., Molino, S., Navajas-Porras, B., Valverde-Moya, A. J., HinojosaNogueira, D., Lopez-Maldonado, A., … Rufian-Henares, J. A. (2021). An in vitro batch fermentation protocol for studying the contribution of food to gut microbiota composition and functionality. *Nature Protocols, 16*(7), 3186–3209. https://doi.org/10.1038/s41596-021-00537-x

Raal, A., Orav, A., Püssa, T., Valner, C., Malmiste, B., & Arak, E. (2012). Content of essential oil, terpenoids and polyphenols in commercial chamomile (Chamomilla recutita L. Rauschert) teas from different countries. *Food Chemistry, 131*(2), 632–638. https://doi.org/10.1016/j.foodchem.2011.09.042

Raja, W., Bera, K., & Ray, B. (2016). Polysaccharides from *Moringa oleifera* gum: Structural elements, interaction with β-lactoglobulin and antioxidative activity. *RSC Advances, 6*(79), 75699–75706. https://doi.org/10.1039/c6ra13279k

Sun, J. R., Li, J. L., Yao, L. L., You, F. F., Yuan, J. F., Wang, D. H., … Gu, S. B. (2023). Synthesis, characterization and antioxidant activity of selenium nanoparticle decorated with polysaccharide from hawthorn. *Journal of Food Measurement and Characterization, 17*, 6125–6134. https://doi.org/10.1007/s11694-023-02124-y

Sun, L., Wang, L., Li, J., & Liu, H. (2014). Characterization and antioxidant activities of degraded polysaccharides from two marine Chrysophyta. *Food Chemistry, 160*, 1–7. https://doi.org/10.1016/j.foodchem.2014.03.067

Tan, Y. W., Li, M. W., Kong, K. Y., Xie, Y. S., Zeng, Z., Fang, Z. F., … Akhtar, M. F. (2020). Antioxidant, anti-inflammatory and antiarthritic potential of *Moringa oleifera* lam: An ethnomedicinal plant of Moringaceae family. *South African Journal of Botany, 128*, 246–256. https://doi.org/10.1016/j.sajb.2019.11.023

Tawfick, M. M., Xie, H., Zhao, C., Shao, P., & Farag, M. A. (2022). Inulin fructans in diet: Role in gut homeostasis, immunity, health outcomes and potential therapeutics. *International Journal of Biological Macromolecules, 208*, 948–961. https://doi.org/10.1016/j.ijbiomac.2022.03.218

Valles-Colomer, M., Falony, G., Darzi, Y., Tigchelaar, E. F., Wang, J., Tito, R. Y., … Raes, J. (2019). The neuroactive potential of the human gut microbiota in quality of life and depression. *Nature Microbiology, 4*(4), 623–632. https://doi.org/10.1038/s41564-018-0337-x

Wang, F., Bao, Y. F., Si, J. J., Duan, Y., Weng, Z. B., & Shen, X. C. (2019). The beneficial effects of a polysaccharide from Moringa oleifera leaf on gut microecology in mice. *Journal of Medicinal Food, 22*(9), 907–918. https://doi.org/10.1089/jmf.2018.4382

Wang, J., & Nie, S. (2019). Application of atomic force microscopy in microscopic analysis of polysaccharide. *Trends in Food Science and Technology, 87*, 35–46. https://doi.org/10.1016/j.ti fs.2018.02.005

Wang, M., & Cheong, K. L. (2023). Preparation, structural characterisation, and bioactivities of fructans: A review. *Molecules, 28*(4), 1613. https://doi.org/10.3390/molecules28041613

Wu, D. T., Fu, Y., Guo, H., Yuan, Q., Nie, X. R., Wang, S. P., & Gan, R. Y. (2021). *In vitro* simulated digestion and fecal fermentation of polysaccharides from loquat leaves: Dynamic changes in physicochemical properties and impacts on human gut microbiota. *International Journal of Biological Macromolecules, 168*, 733–742. https://doi.org/10.1016/j.ijbiomac.2020.11.130

Wu, D. T., Liu, W., Yuan, Q., Gan, R. Y., Hu, Y. C., Wang, S. P., & Zou, L. (2022). Dynamic variations in physicochemical characteristics of oolong tea polysaccharides during simulated digestion and fecal fermentation *in vitro*. *Food Chemistry: X, 14*, Article 100288. https://doi.org/10.1016/j.fochx.2022.100288

Wu, D. T., Nie, X. R., Gan, R. Y., Guo, H., Fu, H., Yuan, Q., & Qin, W. (2020). *In vitro* digestion and fecal fermentation behaviors of a pectic polysaccharide from okra (Abelmoschus esculentus) and its impacts on human gut microbiota. *Food Hydrocolloids, 114*, Article 106577. https://doi.org/10.1016/j.foodhyd.2020.106577

Xu, Y. Q., Liu, N. Y., Fu, X. T., Wang, L. X., Yang, Y., Ren, Y. Y., … Wang, L. B. (2019). Structural characteristics, biological, rheological and thermal properties of the polysaccharide and the degraded polysaccharide from raspberry fruits. *International Journal of Biological Macromolecules, 132*, 109–118. https://doi.org/10.1016/j.ijbiomac.2019.03.180

Yan, S., Pan, C., Yang, X., Chen, S., Qi, B., & Huang, H. (2021). Degradation of Codium cylindricum polysaccharides by H_2O_2-Vc ultrasonic and H_2O_2-Fe^{2+}-ultrasonic treatment: Structural characterization and antioxidant activity. *International Journal of Biological Macromolecules, 182*, 129–135. https://doi.org/10.1016/j.ijbiomac.2021.03.193

Yang, M., Tao, L., Kang, X. R., Li, L. F., Zhao, C. C., Wang, Z. L., … Tian, Y. (2022). Recent developments in Moringa oleifera Lam. polysaccharides: A review of the relationship between extraction methods, structural characteristics and functional activities. *Food Chemistry, X, 14*, Article 100322. https://doi.org/10.1016/j.fochx.2022.100322

Yang, M., Tao, L., Kang, X. R., Wang, Z. L., Su, L. Y., Li, L. F., … Tian, Y. (2023). Moringa oleifera Lam. leaves as new raw food material: A review of its nutritional composition, functional properties, and comprehensive application. *Trends in Food Science & Technology, 138*, 399–416. https://doi.org/10.1016/j.tifs.2023.05.013

Yang, X. Y., Lin, L. Z., & Zhao, M. M. (2023). Preparation, chemical composition, glycolipid- lowering activity and functional property of high-purity polysaccharide from *Moringa oleifera* Lam. leaf: A novel plant-based functional hydrophilic colloid. *Food Hydrocolloids, 142*, Article 108857. https://doi.org/10.1016/j.foodhyd.2023.108857

Yao, W. Z., Liu, M. Y., Chen, X. Y., You, L. J., Ma, Y. X., & Hileuskay, K. (2022). Effects of UV/H_2O_2 degradation and step gradient ethanol precipitation on *Sargassum fusiforme* polysaccharides: Physicochemical characterization and protective effects against intestinal epithelial injury. *Food Research International, 155*, Article 111093. https://doi.org/10.1016/j.foodres.2022.111093

Yu, Y. Y., Zhu, Z. H., Xu, Y. J., Wu, J. J., & Yu, Y. S. (2023). Effects of Lactobacillus plantarum FM 17 fermentation on jackfruit polysaccharides: Physicochemical, structural, and bioactive properties. *International Journal of Biological Macromolecules, 258*(2), 12898. https://doi.org/10.1016/j.ijbiomac.2023.128988

Yuan, D., Li, C., You, L., Dong, H., & Fu, X. (2020). Changes of digestive and fermentation properties of *Sargassum pallidum* polysaccharide after ultrasonic degradation and its impacts on gut microbiota. *International Journal of Biological Macromolecules, 164*, 1443–1450. https://doi.org/10.1016/j.ijbiomac.2020.07.198

Yuan, L., Zhong, Z. C., & Liu, Y. (2020). Structural characterisation and immunomodulatory activity of a neutral polysaccharide from Sambucus adnata Wall. *International Journal of Biological Macromolecules, 154*, 1400–1407. https://doi.org/10.1016/j.ijbiomac.2019.11.021

Zhang, Y. L., Lei, Y., Qi, S. R., Fan, M. X., Zheng, S. Y., Huang, Q. B., & Lu, X. (2023). Ultrasonic-microwave-assisted extraction for enhancing antioxidant activity of Dictyophora indusiata polysaccharides: The difference mechanisms between single and combined assisted extraction. *Ultrasonics Sonochemistry, 95*, Article 106356. https://doi.org/10.1016/j.ultsonch.2023.106356

Zhou, Y., Chen, X., Chen, T., & Chen, X. (2022). A review of theantibacterial activity and mechanisms of plant polysaccharides. *Trends in Food Science & Technology, 123*, 264–280. https://doi.org/10.1016/j.tifs.2022.03.020

Zhu, B. Y., Chen, Y. F., Chang, S. Y., Qiu, H. M., & You, L. J. (2023). Degradation kinetic models and mechanism of isomaltooligosaccharides by hydroxyl radicals in UV/H_2O_2 system. *Carbohydrate Polymers, 300*, Article 120240. https://doi.org/10.1016/j.carbpol.2022.120240